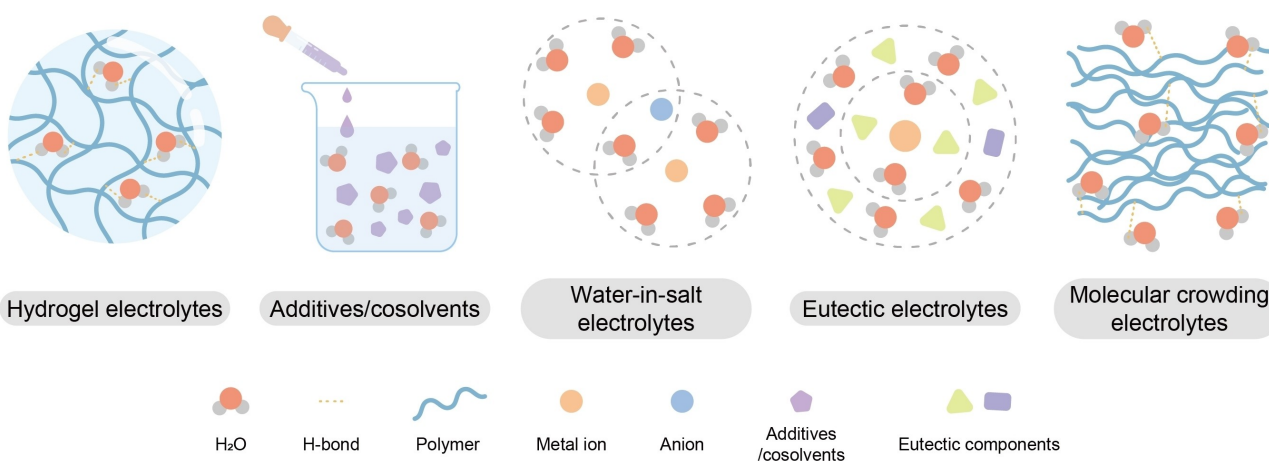




# Green Electrolytes for Aqueous Ion Batteries: Towards High-Energy and Low-Temperature Applications

Eunbin Park,<sup>[a, b]</sup> Jiwon Jeong,<sup>[a, b]</sup> Yung-Eun Sung,<sup>\*[a, b]</sup> and Seung-Ho Yu<sup>\*[c]</sup>



Aqueous battery systems are increasingly recognized for their potential as environmentally friendly next-generation energy storage solutions. However, their commercialization faces challenges due to the need for electrolytes that can operate stably at high voltages and in low-temperatures. Traditional approaches to address these issues often involve materials that compromise the green nature. This review highlights the importance of developing environmentally friendly materials to improve the performance of aqueous electrolytes under high voltage in different types of aqueous electrolytes such as water-

in-salt, molecular crowding electrolytes, eutectic electrolytes and cosolvents. In addition, we review advances in different types of aqueous electrolytes focused on using sustainable materials to achieve stable electrolytes at low-temperature by suppressing water crystallization and lowering the freezing point. By integrating these innovations, we envision a future where aqueous batteries offer both high performance and eco-friendliness, contributing significantly to the development of sustainable energy systems.

## 1. Introduction

The demand for sustainable energy is globally urgent due to climate change. According to environmental regulations announced by the EU, the use of fossil fuels must be reduced, and a 45% reduction in carbon emissions must be achieved by 2030.<sup>[1]</sup> Consequently, Li-ion batteries (LIBs) have been commercialized and used in a wide range of applications. However, the inherent limitations of LIBs are holding back further progress. First of all, the electrolytes used in LIBs are toxic, flammable, and volatile.<sup>[2]</sup> Therefore, during fast charging or in case of accidents, fires can occur rapidly, leading to thermal propagation and even explosions.<sup>[3]</sup> Such incidents release large amounts of toxic gases.<sup>[4]</sup> Since LIBs are comprised of rare metals and toxic materials, there are increasing efforts to prevent the excessive use of these substances by recycling materials.<sup>[5]</sup> Therefore, extensive attention is paid to the development of materials with environmentally friendly substances to ultimately reduce carbon emission and environmental pollutants.<sup>[6]</sup>

Aqueous ion batteries (AIBs), which use water as a solvent for electrolytes, are remarkable alternatives to LIBs. The first aqueous batteries can be traced back to the lead-acid battery developed by Gaston Planté, which laid the foundation for today's widely-used aqueous batteries.<sup>[7]</sup> In 1986, Yamamoto proposed the Zn-MnO<sub>2</sub> battery,<sup>[8]</sup> the first neutral aqueous Zn-ion battery (AZIB), and soon after, in 1994, aqueous Li-ion batteries (ALIBs) emerged,<sup>[9]</sup> accelerating the development of AIBs. This rapid growth can be attributed to the unique characteristics and advantages of aqueous electrolytes. Most importantly, using water as a solvent makes the electrolytes environmentally benign, addressing concerns about pollutant and toxic material emissions associated with conventional LIBs. Additionally, aqueous electrolytes are generally non-flammable

and significantly reduce the danger of releasing toxic gases that could cause air pollution.<sup>[10]</sup> Furthermore, aqueous electrolytes are much more conductive than commercial non-aqueous electrolytes, demonstrating fast kinetics compared to commercial LIB electrolytes.<sup>[11]</sup> Besides, the salts for aqueous electrolytes are far cheaper, and the solvents for aqueous electrolytes are more affordable than organic solvents, offering significant cost advantages.<sup>[12]</sup>

However, using water as the solvent in AIBs has inherent limitations, including a narrow electrochemical stability window (ESW), self-discharge, electrode corrosion and poor temperature stability.<sup>[13]</sup> To overcome these issues, various studies have been conducted for solutions such as electrolyte design,<sup>[14]</sup> separator engineering and electrode modification.<sup>[15]</sup> Among the various solutions, this review thoroughly examines the advances in electrolytes for AIBs, focusing on the sustainable operation of batteries in high-energy and extreme temperature conditions that humankind will face and need to overcome in the future.<sup>[16]</sup> We categorize them into four major types: water-in-salt (WIS) electrolytes, molecular crowding electrolytes, eutectic electrolytes, and cosolvents for aqueous electrolytes. Figure 1a shows studies organized by ESW, a key indicator of high-energy AIBs. Similarly, research on electrolytes for low-temperature applications is classified into hydrogel electrolytes, additives and cosolvents for aqueous electrolytes, WIS electrolytes, and eutectic electrolytes, with both the operating temperature and the freezing point of the electrolytes (Figure 1b). Among those shown in Figure 1, this review mainly discusses the green electrolytes in the context of carbon-neutral trends.<sup>[17]</sup> We classified electrolytes as green if they met one of the following criteria: if a component of the conventional electrolyte composition was replaced with a benign material; if additives with sustainable properties were introduced into the electrolyte; or if the amount of traditionally used toxic and environmentally harmful substances was reduced.

- [a] E. Park, J. Jeong, Y.-E. Sung  
School of Chemical and Biological Engineering, Seoul National University, 1 Gwanak-ro, Seoul 08826, Republic of Korea  
E-mail: ysung@snu.ac.kr
- [b] E. Park, J. Jeong, Y.-E. Sung  
Center for Nanoparticle Research, Institute for Basic Science (IBS), 1 Gwanak-ro, Seoul 08826, Republic of Korea
- [c] S.-H. Yu  
Department of Chemical and Biological Engineering, Korea University, 145 Anam-ro, Seoul 02841, Republic of Korea  
E-mail: seunghoyu@korea.ac.kr

## 2. Green Electrolytes for High-Energy Aqueous Ion Batteries

The main challenge of aqueous ion batteries is creating an internal cell environment that can accommodate the narrow thermodynamic ESW (1.23 V) of aqueous electrolytes, stemming from water's intrinsic thermodynamic properties. Deviations

from this ESW disrupt water stability through anodic oxidation and cathodic reduction, resulting in the production of oxygen and hydrogen.<sup>[18]</sup> As cell pressure increases due to hydrogen evolution reactions (HER), it may induce serious safety issues and degradation of battery performance.

The limited ESW of aqueous electrolytes poses a significant issue, restricting both the energy density of aqueous batteries and the range of viable electrode materials.<sup>[19]</sup> Thus, the ESW, which restricts the voltage range within which battery components can operate without side reactions and water decomposition, should be improved by widening its range. This improvement, in turn, will lead to an increased energy density of the battery following the formula  $E=CV$  (where  $E$  represents energy,  $C$  is capacity, and  $V$  is the operating voltage window).

## 2.1. Water-in-Salt Electrolytes

In order to widen the narrow ESW of aqueous electrolytes, electrolyte concentrations should be increased so that the salt surpass the solvent in both weight and volume percentages. These so-called “water-in-salt” electrolytes induce the formation of passivating layers on the electrodes and broaden the ESW, leading to higher energy density and reduced side reactions in aqueous ion batteries. These passivating layers function as solid-electrolyte interphase (SEI) in aqueous electrolytes, a concept that has traditionally applied only to organic electrolytes and now newly introduced for aqueous electrolytes.<sup>[20]</sup> The SEI layer, which is primarily formed during the first few cycles, is crucial for battery performance as it passivates the interface between anode and electrolyte, preventing side reactions and ensuring efficient ion transport. For optimal performance, the

SEI needs to be not only uniform but also mechanically stable to withstand the stresses caused by volume changes in anode materials during cycling. This stability helps maintain the integrity of the SEI layer and reduce electrolyte consumption, which ultimately enhances the battery’s longevity and performance.<sup>[21]</sup>

In addition to the formation of SEI layer, several other factors also contribute to the widening of the ESW in WIS electrolytes. These factors include reduced water activity, altered solvation structure and enhanced ion-pairing interactions, all of which play a crucial role in stabilizing the electrolyte and expanding the operating voltage window.

In previous studies, conventional aqueous electrolytes consisted of more than 70 wt% of water.<sup>[22]</sup> There was no chance for any protective layer to form because decomposition products from the electrolytes were not able to deposit as a solid state on the electrodes. Therefore, the maximum voltage was limited to 1.5 V in ALIBs, and continuous HER and oxygen evolution reaction (OER) led to destructive self-discharge.<sup>[9]</sup>

However, in 2015, Suo. et al. first reported the concept of WIS in ALIBs by adding 21 m (mol kg<sup>-1</sup>) of lithium bis(trifluoromethane sulfonyl)imide (LiTFSI), decreasing water component to 14.2 wt%.<sup>[20]</sup> By sacrificing electrolyte during the initial cycles, protective layer was produced and expanded the ESW to 3.0 V (Figure 2a). Also, as the salt concentration increased to 21 m, the number of free water molecules per Li<sup>+</sup> decreased from 4 to 2.6 and Li<sup>+</sup> solvation sheath structure was modified by TFSI<sup>-</sup> invasion (Figure 2b). This structure modification led to the formation of a LiF-rich interphase between the anode and electrolyte, similar to the SEI layer on the anode. This LiF layer, created by the reduction of TFSI<sup>-</sup>, prevents HER by forbidding electronic conduction while allowing Li<sup>+</sup> con-



Eunbin Park received her Bachelor of Science degree from RWTH Aachen University, Germany. She is currently pursuing her Ph.D. in the School of Chemical and Biological Engineering at Seoul National University. Her research is mainly focused on aqueous ion batteries and Li metal batteries.



Jiwon Jeong received her B.S. degree in the department of Chemical and Biological Engineering at Seoul National University, where she is currently pursuing her Ph.D. Her current research interests focus on aqueous ion batteries and Li metal batteries.



Yung-Eun Sung received his Ph.D. degree in chemistry from the University of Illinois at Urbana-Champaign, USA. He completed post-doctoral studies in Prof. Allen Bard's laboratory at the University of Texas at Austin, USA. He started as an assistant professor at the Gwangju Institute of Science and Technology in 1998. He moved to Seoul National University in 2004 and became a professor in the Department of Chemical and Biological Engineering in 2008. He also became an associate director at the Center for Nanoparticle Research, Institute for Basic Science (IBS) in 2018. His research interests include electrochemical energy conversion and storage devices.



Seung-Ho Yu is an associate professor in the Department of Chemical and Biological Engineering at Korea University and concurrently holds a position as a professor in the Department of Battery-Smart Factory at Korea University. His current research focuses on material design and revealing reaction mechanisms for (post) Li-ion batteries.

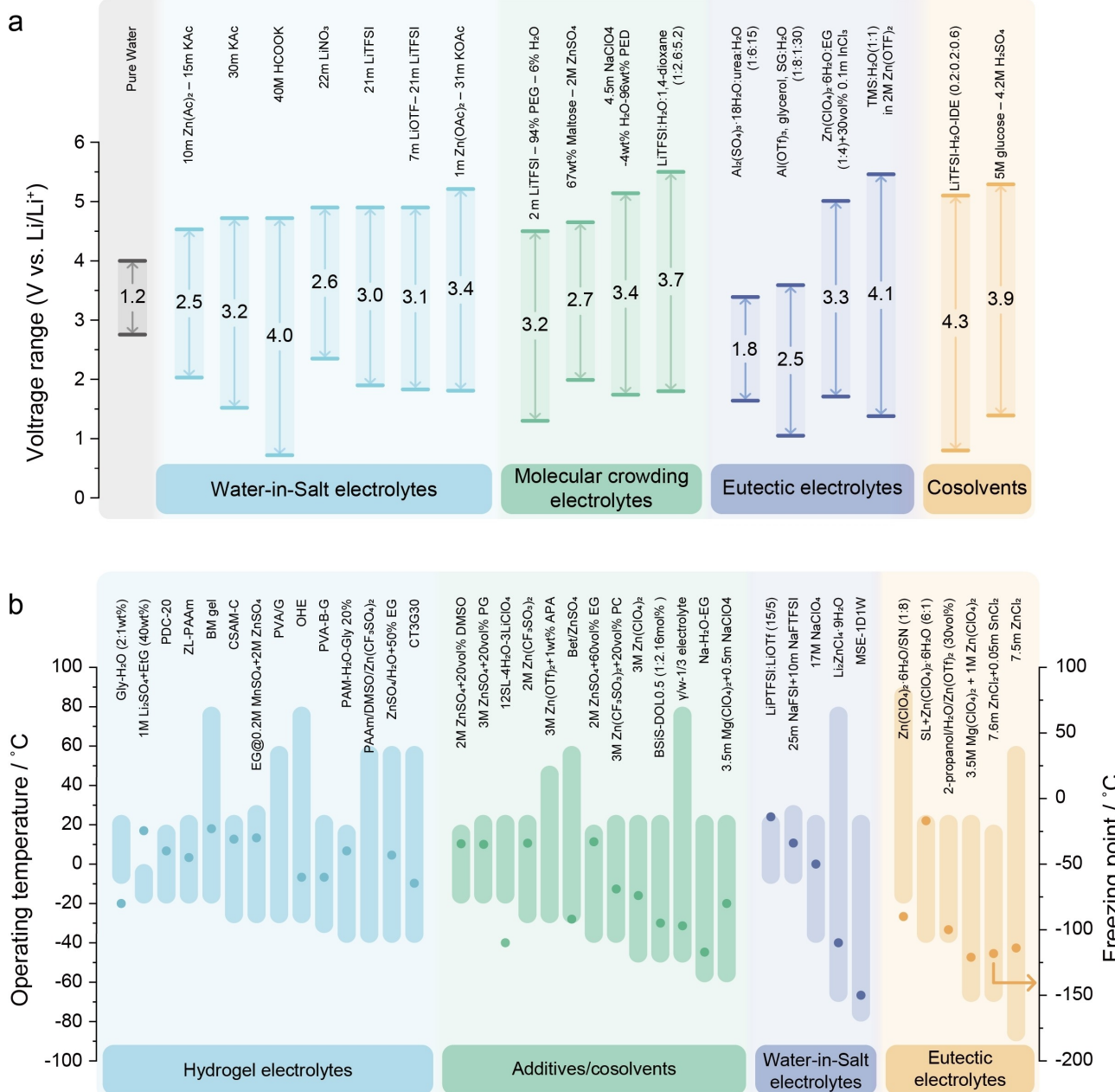


**Figure 1.** Overview of aqueous electrolytes from recent studies: (a) The reported ESWs of various aqueous electrolytes, categorized into four types—Water-in-Salt electrolytes, molecular crowding electrolytes, eutectic electrolytes, and cosolvents. (b) The operating temperature ranges and freezing points of the reported aqueous electrolytes, categorized into four types—hydrogel electrolytes, additives/cosolvents, Water-in-Salt electrolytes, and eutectic electrolytes.

duction. Following this work, extensive WIS electrolytes (21–55 m) research utilizing the concept of anion reduction have been reported.<sup>[22]</sup> However, LiTFSI poses toxicity risks to the skin and nervous system and also contributes to acute aquatic hazards.<sup>[23]</sup> Therefore, its harmful environmental impacts necessitate the exploration of safer alternatives.

Researchers have sought greener anions that dissolve well in water to replace perfluorinated reagents. Although Li-based salts typically have low solubility in water, several fluorine-free salts have been discovered that dissolve effectively and reduce well to form a robust SEI layer in aqueous electrolytes. For instance, a 22 m LiNO<sub>3</sub> solution was reported as an eco-friendly

ALIB electrolyte with high water solubility and cost-effectiveness, offering a wide ESW of 2.55 V. Unlike conventional room-temperature lithium nitrate aqueous electrolytes, it achieves a super-concentrated solution state with a salt to water molar ratio of 1:2.35 at 35 °C. Molecular dynamics (MD) simulations (Figure 2c) and atomic pair-distribution function analysis of high-energy X-ray diffraction (XRD) data were employed to validate the formation of a self-assembled (Li<sup>+</sup>(H<sub>2</sub>O)<sub>n</sub>) polymer-like aggregation chain, which realizes higher thermodynamic (high salt concentration) and kinetic (protective SEI layer) stabilities. This study elucidates the thermodynamic and kinetic

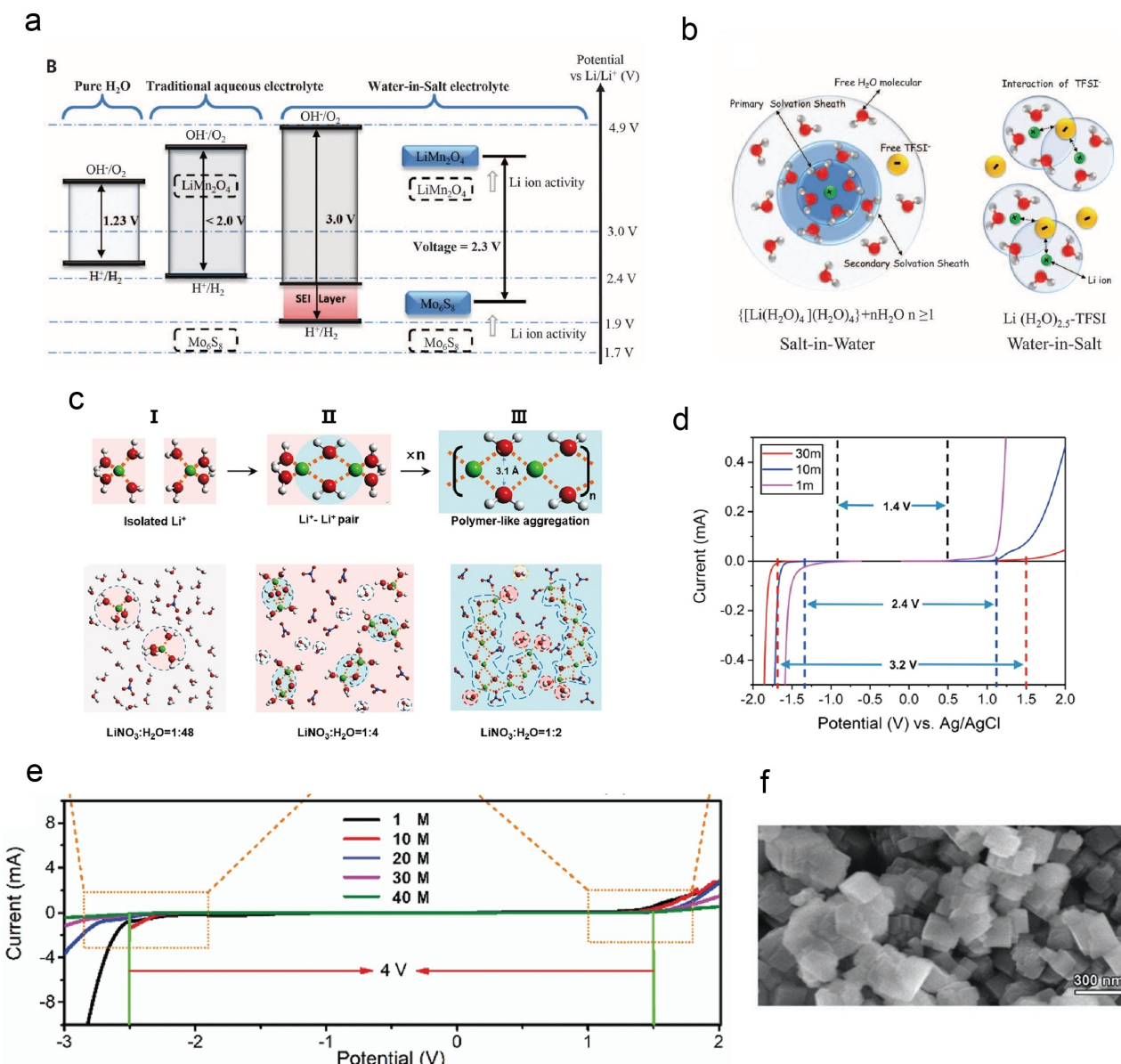


**Figure 2.** (a) Expanded electrochemical stability window (ESW) of water in salt electrolytes. (b) Schematic illustration of  $\text{Li}^+$  primary solvation sheath for diluted solutions and water in salt solutions. Reproduced with permission.<sup>[20]</sup> Copyright 2015, AAAS. (c) Illustration and MD simulation of local structure evolution of  $\text{LiNO}_3$  aqueous solution with the increasing concentration. Reproduced with permission.<sup>[24]</sup> Copyright 2018, Elsevier. (d) Extended ESW confirmed by linear sweep voltammetry (LSV) curves recorded at  $1 \text{ mVs}^{-1}$  in 1, 10, and 30 m KAc electrolytes. Reproduced with permission.<sup>[25]</sup> Copyright 2018, American Chemical Society (e) LSV curves of the HCOOK electrolytes at  $10 \text{ mVs}^{-1}$ . (f) SEM image of  $\text{KTi}_2(\text{PO}_4)_3$  anode. Reproduced with permission.<sup>[27]</sup> Copyright 2019, Royal Society of Chemistry.

factors and their respective impact on the electrochemical behaviors.<sup>[24]</sup>

Furthermore, there is another study which eliminates the concerns of using highly fluorinated Li salts, which are costly and toxic, by utilizing an alternative acetate-based electrolyte.

Leonard et al. applied highly soluble 30 m potassium acetate (KAc) as a salt for aqueous K-ion batteries (KIBs), extending the ESW to 3.2 V (Figure 2d).<sup>[25]</sup> The 30 m KAc exhibits superior conductivity over LiTFSI and other fluorinated salts, such as potassium hexafluorophosphate ( $\text{KPF}_6$ ) and potassium bis(trifluoromethanesulfonyl)imide (KTFSI).<sup>[26]</sup> This enhanced

conductivity may arise from the weak Lewis acidity of K ions and the inherent properties of the acetate salt. It realizes the reversible operation of the  $\text{KTi}_2(\text{PO}_4)_3$  anode in aqueous electrolytes over 10000 cycles at  $1 \text{ Ag}^{-1}$ , which shows an exceptionally superior performance, presenting the potential of eco-friendly, high energy density KIBs.<sup>[25]</sup> However, it still lacks stable negative potential, hindering practical application.

Beyond acetate-based electrolytes, further research on WIS for KIBs has been conducted. Liu et al. proposed a 40 M ( $\text{mol L}^{-1}$ ) potassium formate (HCOOK), which is both economic and environmentally friendly.<sup>[27]</sup> Furthermore, with this electro-

lyte, a wide ESW of 4 V (−2.5 V to 1.5 V vs. Ag/AgCl) was realized (Figure 2e) and displayed a promising capacitance of 321 F g<sup>−1</sup> at 5 A g<sup>−1</sup> with activated carbon-based positive electrodes. Solvation structure of water is altered as the majority of water molecules interact with K ion via van der Waals force, reducing the number of free water clusters. This, in turn, protects the electrodes by suppressing the evolution of hydrogen and oxygen gases. Additionally, compared to the CH<sub>3</sub>COK (KAc)-based electrolytes mentioned above,<sup>[25]</sup> the HCOOK-based electrolyte with a salt to water ratio of 1:1.38 can reach lower negative discharge potential of −2.4 V vs. Ag/AgCl. It is a crucial factor that leads to higher energy density and power density, enabling a reversible capacity of 15 mAh g<sup>−1</sup> at 0.1 A g<sup>−1</sup> with KTi<sub>2</sub>(PO<sub>4</sub>)<sub>3</sub> anode (Figure 2f). In addition, a 10 M HCOOK solution exhibits a higher ionic conductivity of 130 mS cm<sup>−1</sup>, which exceeds that of other fluorinated imide-based WIS electrolytes and 10 M KAc-based electrolytes (90 mS cm<sup>−1</sup>), which is attributed to the weaker Lewis acidity of the formate salt.

## 2.2. Water-in-Bisalt Electrolytes

Although WIS electrolytes have expanded ESW to a great extent by forming robust SEI on the anode through decomposition of salt anions, there still remains a need for improved energy density to make aqueous ion batteries more practical for real-world applications. Therefore, for wider ESW, we need more concentrated electrolytes capable of minimizing the presence of free water molecules by more precisely regulating the solvation sphere of metal ions. However, ALIB employing the aforementioned 21 m LiTFSI in water, or LiTFSI (H<sub>2</sub>O)<sub>2.6</sub> electrolyte have already reached the saturation limit of salt, making it impossible to increase the salt concentration and further construct SEI anymore.<sup>[20]</sup>

Nevertheless, researchers discovered a new way to achieve higher concentration electrolytes by adopting the strategy of molten salt mixtures.<sup>[28]</sup> “Hydrate melt”, which refers to saturated hydrated salt, can dissolve additional unhydrated salt with similar chemical properties, forming molten salt mixtures. Inspired by this mechanism, Suo et al. introduced second salts (7 m lithium trifluoromethanesulfonate (LiOTf)) into the original “water-in-salt” electrolyte (21 m LiTFSI), leading to the emergence of “water-in-bisalt” (WIBS) electrolytes.<sup>[29]</sup> In comparison to the previous 21 m LiTFSI electrolyte, WIBS with 21 m LiTFSI and 7 m LiOTf realized a higher salt concentration (28 m) and consequently, a wider ESW (3.1 V) at room temperature. Also, the number of free water molecules per Li<sup>+</sup> decreased from 2.6 to about 2.0, as verified by MD simulations (Figure 3a), and the HER potential decreased from 1.9 V in WIS to 1.83 V in WIBS electrolyte (Figure 3b), resulting in denser and durable SEI to be formed before HER. By reducing water activity, it enabled a LiMn<sub>2</sub>O<sub>4</sub>/C-TiO<sub>2</sub> full Li-ion cell to operate at a high voltage of 2.1 V and achieve an energy density of 100 Wh kg<sup>−1</sup>. This work paved the way for incorporating a second or even additional salts into WIS, resulting in superior high energy density aqueous rechargeable batteries.

However, costly fluorinated salts are still used as WIBS electrolytes, resulting in a corrosive internal cell environment. In contrast, ideal WIBS electrolytes should be environmentally sustainable, cost-effective and offer high water solubility. As a promising alternative to fluorine-based WIBS electrolytes, zinc acetate (Zn(Ac)<sub>2</sub>) was newly adopted as a green salt for AZIBs. AZIBs utilizing Zn<sup>2+</sup> as the charge carrier have attracted great interest due to their low redox potential (−0.76 V versus standard hydrogen electrode (SHE)), high energy density, plentiful Zn resources and affordability.<sup>[12b]</sup> Chen et al. employed mixed 1 m Zn(Ac)<sub>2</sub>+31 m KAc solution to address concerns about toxicity and cost of perfluorinated reagents. It demonstrated a wide ESW of 3.4 V, enabling successful operation of Zn/MnO<sub>2</sub> full cell with a high discharge capacity of 304.6 mAh g<sup>−1</sup>.<sup>[30]</sup> The cell has distinct storage mechanisms for anode and cathode respectively due to the mild alkalinity of the electrolyte with a pH of 9.76 (Figure 3c). On the Zn anode side, a Zn<sup>2+</sup> plating/stripping reaction occurs and on the MnO<sub>2</sub> cathode side, a proton intercalation/deintercalation process occurs.

On the other hand, due to the solubility limitation of Zn(Ac)<sub>2</sub> (1.6 m),<sup>[30]</sup> it inevitably lowers the population of Zn<sup>2+</sup> carrier ions in electrolytes and results in high overpotential and poor rate performance.<sup>[32]</sup> Hence, a new approach was needed that could handle both the Zn ion deficiency and the reliance on halogen salts. One effective solution involved utilizing the hydrotropic solubilization strategy. Hydrotropic solubilization method is frequently observed in the pharmaceutical industry, which allows poorly water-soluble drugs to dissolve well in water by forming soluble complexes, double salts, or interactions with hydrotropic agents.<sup>[33]</sup>

For example, Figure 3d demonstrates the addition of 15 m KAc as a hydrotropic solubilization agent effectively dissolving 10 m Zn(Ac)<sub>2</sub> in water. To confirm the versatility of this method in enhancing Zn cycling reversibility, Lu' group explored three different highly concentrated Zn(Ac)<sub>2</sub> electrolytes, based on KAc, urea, and acetamide, respectively.<sup>[31]</sup> In previous studies, supersaturated zinc acetate solution had a residual hydrophobic −CH<sub>3</sub> shell due to bidentate chelation with Zn<sup>2+</sup> and acetate ion, hindering further dissociation of zinc acetate. However, by introducing the aforementioned hydrotropic agents, they established strong coordination with Zn<sup>2+</sup>, displacing the acetate's binding sites and ensuring solubility through their additional hydrophilic coordination sites. Fourier-transform infrared spectroscopy (FTIR) spectra clarify solvation structure between Zn ion and acetate by the difference between the antisymmetric  $\nu_{as}$  ( $\approx 1,550 \text{ cm}^{-1}$ ) and the symmetric  $\nu_s$  ( $\approx 1,400 \text{ cm}^{-1}$ ) wavenumbers (Figure 3e). HSE-10 m (X m Zn(Ac)<sub>2</sub>-15 m KAc (X = the molality of Zn(Ac)<sub>2</sub>), denoted HSE-X m) exhibits the largest  $\Delta$  value compared with solid Zn(Ac)<sub>2</sub>·2H<sub>2</sub>O, 1.6 m Zn(Ac)<sub>2</sub> and HSE-X m (X = 2, 5, 8), indicating increasing value of monodentate/bidentate bonding of acetate (Figure 3f). Consequently, HSE-10 m enables Zn/pyrene-4,5,9,10-tetraone (PTO) full cell to operate stably over 4000 cycles at 10 C. However, non-fluorinated electrolytes still encounter the limitations of narrower ESW and the resulting lower energy density compared to fluorinated electrolytes. A more fundamental issue

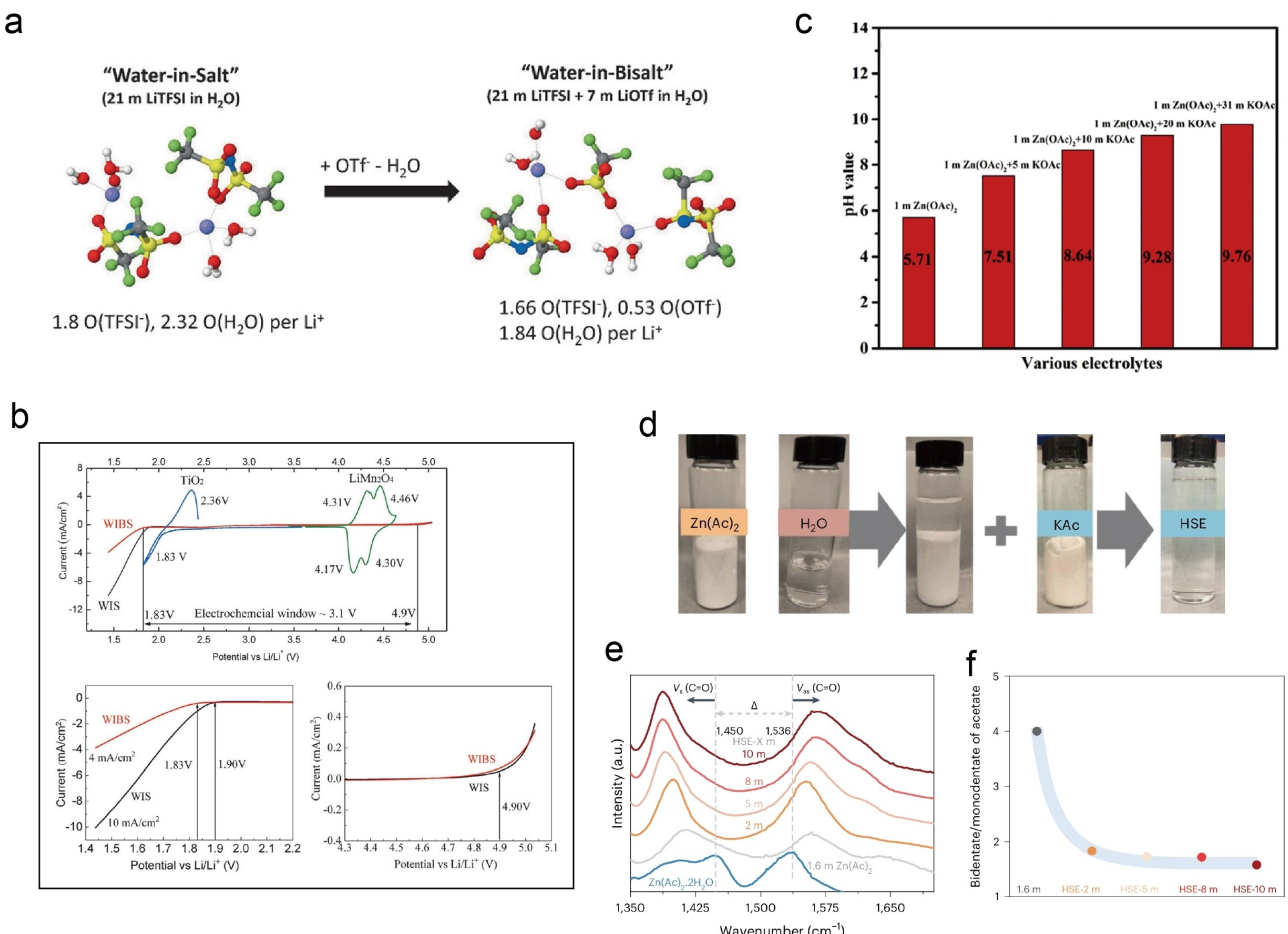


**Figure 3.** (a) Schematic illustration of the Li<sup>+</sup> first coordination shell modification by adopting 7 m LiOTf, obtained by MD simulation. (b) Cyclic voltammetry (CV) of 21 m LiTFSI (WIS) and 21 m LiTFSI + 7 m LiOTf (WIBS) electrolytes. Reproduced with permission.<sup>[29]</sup> Copyright 2016, Wiley-VCH. (c) Increasing pH value of the alkaline KOAc solution. Reproduced with permission.<sup>[30]</sup> Copyright 2020, Elsevier. (d) Method of achieving highly concentrated zinc acetate by addition of 15 m KAc as the hydrotropic solubilization agent. (e) FTIR spectra of different HSE-Xm electrolytes. (f) Proportion of bidentate to monodentate acetate determined through MD simulation. Reproduced with permission.<sup>[31]</sup> Copyright 2023, Springer Nature.

is that, while increasing salt concentration through WIS and WIBS effectively regulates the water solvation structure, it is costly and has limited practical applicability.

### 2.3. Molecular Crowding Electrolytes

Researchers explored new methods for developing greener and more affordable electrolytes and discovered an interesting phenomenon known as "molecular crowding", which is frequently observed in living cells. Intracellular environment of living cells is crowded state with macromolecules, cell organelles and also small hydrophilic molecules such as amino acids, sugars and urea. These molecules constrain free movement of water by forming hydrogen bonds with water molecules, forming hydration structure. Therefore, the dense environment caused by crowding agents alters the solvent properties and decreases water activity.<sup>[34]</sup> By employing this new phenomenon, it becomes feasible to develop high-voltage aqueous electrolytes even at low molar concentrations despite the

challenges posed by WIS electrolytes, which undermine ionic conductivity due to high viscosity caused by high salt concentrations.

In 2020, Lu's group introduced poly(ethylene glycol) (PEG) as a molecular crowding agent with a dilute 2 m LiTFSI solution, which demonstrated a wide ESW of 3.2 V even though it has low Li salt concentration. This was made possible by trapping water molecules within a PEG network through hydrogen bonding, effectively suppressing HER and OER, illustrated by MD simulation (Figure 4a). As a result, ESW increases with higher PEG concentrations (Figure 4b). Moreover, PEG is inexpensive, non-toxic and also resulting molecular crowding aqueous electrolyte (2 m LiTFSI–94%PEG–6%H<sub>2</sub>O) exhibits non-flammable properties, as verified by flammability test (Figure 4c). This safe and green electrolyte achieves a stable energy density between 75 and 110 Wh kg<sup>-1</sup> in full Li<sub>4</sub>Ti<sub>5</sub>O<sub>12</sub>/LiMn<sub>2</sub>O<sub>4</sub> cells over 300 cycles.<sup>[35]</sup>

Moreover, Nian et al. further confirmed the molecular crowding concept by adopting 1,4-Dioxane (DX) as a molecular overcrowding agent in LiTFSI-based electrolyte.<sup>[36]</sup> This research

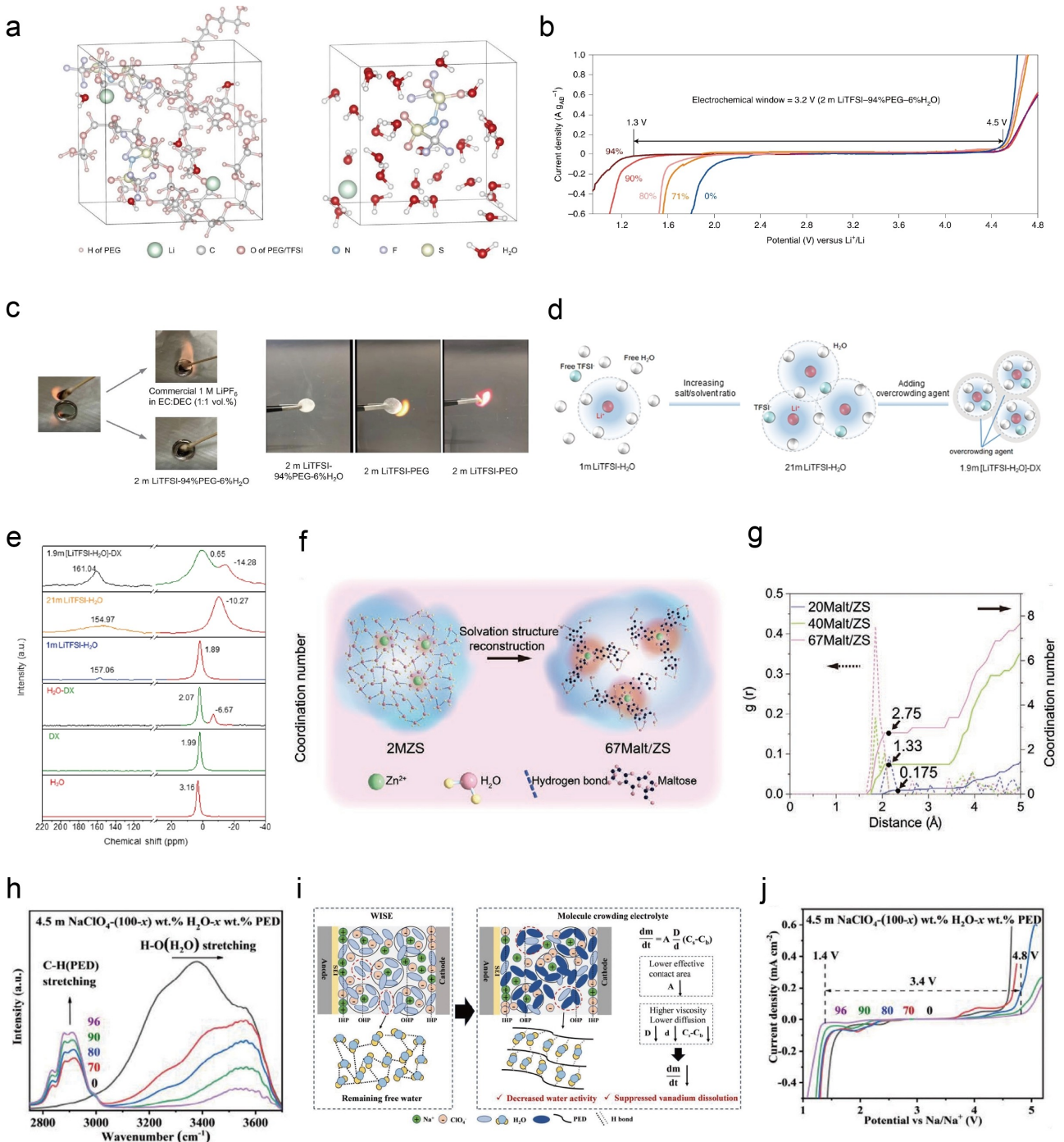


**Figure 4.** (a) Schematic snapshot illustration of 2 m LiTFSI-94%PEG-6%H<sub>2</sub>O and 2 m LiTFSI-H<sub>2</sub>O electrolyte obtained by MD simulations. (b) Widened ESW with increasing PEG concentrations for 2 m LiTFSI-x PEG-(1-x) H<sub>2</sub>O solutions ( $x = 0, 71, 80, 90, 94\%$ ). (c) Flammability test of different electrolytes. Reproduced with permission.<sup>[35]</sup> Copyright 2020, Springer Nature. (d) Schematic illustration of solvation structures of 1 m LiTFSI, 21 m LiTFSI-H<sub>2</sub>O, and 1.9 m [LiTFSI-H<sub>2</sub>O]-DX towards molecular crowding electrolyte. (e) <sup>17</sup>O NMR spectra of various solvents and electrolytes. Reproduced with permission.<sup>[36]</sup> Copyright 2021, American Chemical Society. (f) Microscopic configuration of environment transformation after introducing 67 Malt/ZS electrolyte. (g) Radial distribution function for Zn<sup>2+</sup>-Maltose pairs under different concentrations of electrolytes. Reproduced with permission.<sup>[37]</sup> Copyright 2022, Wiley-VCH. (h) FTIR spectra of 4.5 m NaClO<sub>4</sub> in electrolytes composed of (100-x) wt % H<sub>2</sub>O and x wt % PED ( $x = 0, 70, 80, 90, 96$ ) across the 2750–3700 cm<sup>-1</sup> range. (i) Schematic illustration depicting multiple functions of PED as molecular crowding agents. (j) LSV curves of the 4.5 m NaClO<sub>4</sub>-(100-x) wt % H<sub>2</sub>O-x wt % PED ( $x = 0, 70, 80, 90, 96$ ) at 5 mV s<sup>-1</sup>. Reproduced with permission.<sup>[38]</sup> Copyright 2024, Wiley-VCH.

is meaningful for reducing LiTFSI salt concentration from 21 m<sup>[20]</sup> to 1.9 m compared to previous WIS studies, alleviating both toxicity and cost of electrolytes. Overcrowded solvation

structure is formed through hydrogen bonding between DX and water, by decreasing outward electrostatic attractions of nearby ions while enhancing inward electrostatic attractions

(Figure 4d). DX has low dielectric constant ( $\epsilon=2.25$  at  $25^\circ\text{C}$ ) as a nonpolar molecule, so it has low solvating ability for LiTFSI. However, it has relatively good solubility in  $\text{H}_2\text{O}$ , 72 times higher than in LiTFSI. Hence, this allows DX to form over-crowded solvation structure without disturbing  $\text{TFSI}^-\text{Li}^+(\text{H}_2\text{O})_x$  solvation structure. In this environment,  $\text{H}_2\text{O}$  acts as hydrogen bond donor and DX acts as hydrogen bond acceptor, as supported by nuclear magnetic resonance (NMR) spectroscopy results (Figure 4e). The 1.9 m [LiTFSI- $\text{H}_2\text{O}$ ]-DX electrolyte creates a dense LiF-rich SEI, realizing a wide ESW of 3.7 V in ALIBs and delivering much higher electrochemical performance than WIS electrolytes. It shows outstanding  $\text{Li}^+$  intercalation and extraction properties, along with long-term cycling stability, retaining 88.5% of its capacity after 200 cycles at 0.57 C in  $\text{Li}_4\text{Ti}_5\text{O}_{12}/\text{LiMn}_2\text{O}_4$  full cells.

In addition, maltose-based hybrid solution was reported, employing similar molecular crowding strategy in aqueous Zn-ion batteries. Maltose is green, inexpensive multihydroxyl organic material. It was mixed with 2 M  $\text{ZnSO}_4$  (ZS) base electrolytes to form 67Malt/ZnSO<sub>4</sub>, where 67 refers to mass fraction of saccharide. Maltose dissolves easily in aqueous solutions due to its abundant hydroxyl groups. It interrupts both hydrogen bonding and  $\text{Zn}^{2+}$  solvation structure, establishing new large  $\text{Zn}^{2+}$  solvation shell (Figure 4f). As a result, 67Malt/ZS electrolyte constructs massive solvation sheath by hydrogen bonds between  $\text{H}_2\text{O}$  molecules and hydroxyl groups of maltose, leading to increased coordination numbers of maltose to Zn ion from 1.33 to 2.75 (Figure 4g). Zn/NH<sub>4</sub>V<sub>4</sub>O<sub>10</sub> (NVO) full batteries with 67Malt/ZS electrolyte demonstrates 84.2% of capacity retention at 50 mA g<sup>-1</sup> over 400 cycles, ensuring structural stability of NVO cathode.<sup>[37]</sup>

Besides Zn-based systems, Ding et al. recently reported polyethylene glycol dimethyl ether (PED) as a nonflammable molecular crowding agent for aqueous Na-ion batteries (ANIBs). 4.5 m  $\text{NaClO}_4$ -4 wt %  $\text{H}_2\text{O}$ -96 wt % PED electrolyte disrupts original hydrogen bond by forming new hydrogen bond networks between PED and water, reducing water activity. FTIR spectra support this fact, showing a blue shift in the H-O stretching band, which indicates enhanced interaction between water and PEO (Figure 4h). Another decisive factor is a dense arrangement of long-chain PED, which traps water molecules within the PED network physically via hydrogen bonding, illustrated in Figure 4i. The electrolyte shows wide ESW of 3.4 V by shifting HER potential to 1.4 V (vs.  $\text{Na}/\text{Na}^+$ ) and OER potential to 4.8 V (vs.  $\text{Na}/\text{Na}^+$ ), surpassing stability range of pure water solvent (2.29–3.53 V vs.  $\text{Na}/\text{Na}^+$ ) (Figure 4j). As a result, it enables stable  $\text{NaTi}_2(\text{PO}_4)_3/\text{Na}_3\text{V}_2(\text{PO}_4)_3$  full cell operation at 1 C with capacity retention of 74% over 100 cycles, significantly suppressing vanadium dissolution.<sup>[38]</sup>

#### 2.4. Eutectic Electrolytes

Eutectic solvents are composed of a mixture of two or three substances, where complex anions and cations usually arise from their strong intermolecular interactions.<sup>[39]</sup> In eutectic mixtures, the melting point is significantly reduced to attain a

liquid phase, even though individual components have high melting points, as shown in Figure 5a. They are ideal for large-scale applications because they have a nearly 100% utilization rate of raw reagents, eliminating the need for additional processing. Eutectic electrolytes are mainly formed through three types of interactions: hydrogen bonding, Lewis acid-base interactions, and van der Waals forces.<sup>[40]</sup>

Feng et al. developed eutectic electrolytes with 20% volume ratio of recyclable dimethyl sulfoxide (DMSO) in 2 M  $\text{ZnSO}_4$  electrolyte, based on hydrogen-bond interactions between DMSO and water molecules. Due to its higher binding energy to Zn ion, DMSO confines the typical solvation sheath of Zn ion ( $[\text{Zn}(\text{H}_2\text{O})_6]^{2+}$ ) (Figure 5b) and hinders side reactions caused by water decomposition. More specifically, the  $[\text{Zn}(\text{H}_2\text{O})_m(\text{DMSO})_n]^{2+}$  structure is formed by S=O-H-O hydrogen bonding, which induces fine-grained Zn (002)-plane deposition, as confirmed by XRD results (Figure 5c). Moreover, in 20 DMSO hybrid electrolyte, the freezing point is lowered to  $-34.51^\circ\text{C}$  and the ionic conductivity is increased, resulting in improved cycle stability of  $\text{Zn}/\text{MnO}_2$  full cell over 3000 cycles at 10 C under 20  $^\circ\text{C}$ , enabling a specific capacity of 140 mA h g<sup>-1</sup>.<sup>[41]</sup>

Another hydrogen bonding type eutectic electrolyte was designed by Zhong et al., adopting tetramethylene sulfone (TMS) as an alternative to DMSO, which has lower toxicity and reduced skin permeability. TMS acts as hydrogen-bond acceptor (HBA) and participates in the primary solvation shell of  $\text{Zn}^{2+}$ , enhancing ESW to 4.08 V. Hydrogen bonding results in solvent co-intercalation ( $(\text{Zn-TMS})^{2+}$ ) mechanism, which induces the formation of TMS pillars and creates abundant  $\text{Zn}^{2+}$  binding sites (Figure 5d), thereby stabilizing NVO structure. TMS also preferentially adsorbs onto the Zn anode and thicken double electric layer (EDL) buffer, inhibiting 2D diffusion of  $\text{Zn}^{2+}$  and Zn dendrite growth. Consequently, the Zn/NVO full cell demonstrates a high specific capacity of up to 515.6 mA h g<sup>-1</sup>, even at a low current density of 0.2 A g<sup>-1</sup> for more than 40 days.<sup>[42]</sup>

Furthermore, Lewis acid-base interactions-based eutectic electrolyte was also reported by Lu et al., employing urea-based hydrated eutectic electrolytes. Mixtures of  $\text{Al}_2(\text{SO}_4)_3 \cdot 18\text{H}_2\text{O}$ , urea and pure water in 1:6:15 molar ratio (labeled as AU15) create a transparent and uniform liquid with green, low-cost properties, weak corrosiveness and high ionic conductivity. Urea serves as a Lewis base through lone-pair electrons of its oxygen atoms, interacting with  $\text{Al}^{3+}$  and changing the primary solvation shell of  $\text{Al}^{3+}$ . As a result, urea replaces water in the solvation shell, forming  $[\text{Al}(\text{Urea})_x(\text{H}_2\text{O})]^{3+}$ , which confines water activity, as illustrated in Figure 5e. This electrolyte enabled  $\text{Zn}/\text{V}_2\text{O}_5$  full cell to reach high discharge capacity of 250 mA h g<sup>-1</sup> and long cycle retention of 1500 cycles.<sup>[43]</sup>

Recently, eutectic electrolyte made up of  $\text{Al}(\text{OTf})_3$ , glycerol (Gly), sodium beta-glycerophosphate pentahydrate (SG) in a molar ratio of 1:8:1, with 30 vol% water (denoted as HEE30), was also effectively utilized in Al-ion batteries. Glycerol, used as main ingredient for the electrolyte is a valuable biodegradable green solvent with low toxicity ( $\text{LD}_{50}$  (oral rat) = 12600 mg kg<sup>-1</sup>) and is non-flammable.<sup>[44]</sup> Similar to the mechanism of aforementioned eutectic solvents, hydrogen bonding

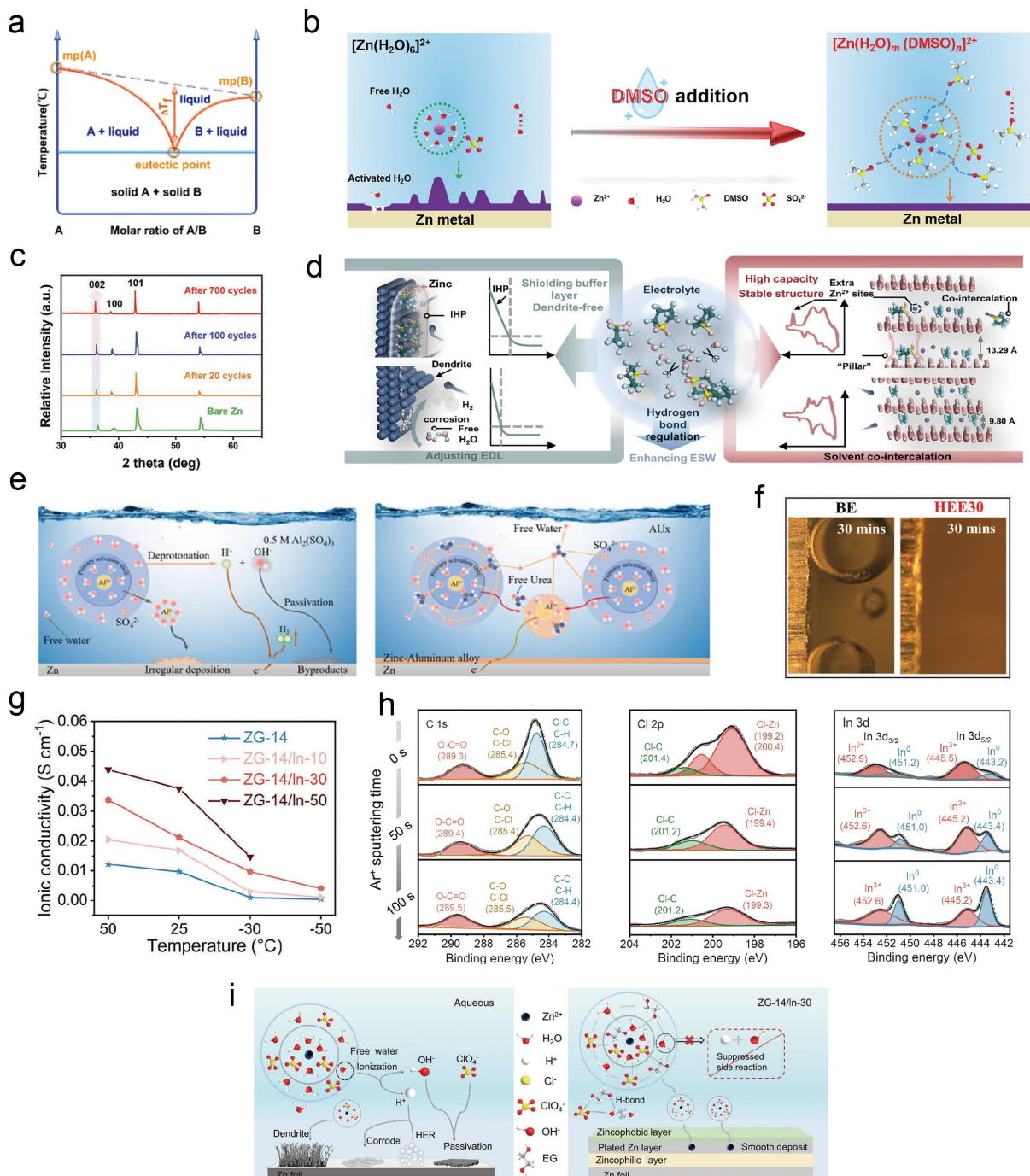


**Figure 5.** (a) Phase diagram of binary-component eutectic electrolytes. Reproduced with permission.<sup>[40]</sup> Copyright 2012, Royal Society of Chemistry. (b) Schematic illustration of  $\text{Zn}^{2+}$  solvation structure before and after applying DMSO hybrid electrolytes. (c) X-ray diffraction (XRD) results of Zn metal in 20 vol% DMSO after various cycles at  $1.0 \text{ mA cm}^{-2}$ . Reproduced with permission.<sup>[41]</sup> Copyright 2021, Wiley-VCH. (d) Schematic illustration of impact of applying triple-function TMS on cell. Reproduced with permission.<sup>[42]</sup> Copyright 2023, Wiley-VCH. (e) Schematic illustration of  $\text{Al}^{3+}$  solvation structure modification after introduction of urea. Reproduced with permission.<sup>[43]</sup> Copyright 2024, Elsevier. (f) In-situ monitoring of HER on Al foil, utilizing HEE30 eutectic electrolyte and 1 M  $\text{Al}(\text{OTf})_3$  bare electrolyte at  $0.2 \text{ mA cm}^{-2}$ . Reproduced with permission.<sup>[45]</sup> Copyright 2024, Wiley-VCH. (g) Ionic conductivity of various hydrated eutectic electrolytes at different temperatures with varying volume fractions of  $\text{InCl}_3$ . (h) XPS C 1s, Cl 2p and In 3d spectra of cycled Zn electrodes with ZG-14/ln-30 eutectic electrolytes. (i) Schematic illustration of  $\text{Zn}^{2+}$  solvation structure and reactions in aqueous solution (left) and ZG-14/ln-30 hybrid eutectic solution (right). Reproduced with permission.<sup>[46]</sup> Copyright 2024, Wiley-VCH.

between glycerol and water is strengthened in the electrolyte, excluding active  $\text{H}_2\text{O}$  from  $\text{Al}^{3+}$  with assistance of SG as an extra crosslinking additive. In turn, HER is suppressed as shown in Figure 5f, and freezing point of the electrolyte is lowered to

$-20^{\circ}\text{C}$ . This electrolyte enables Al/Prussian white (PW) full cell to operate stably for more than 100 cycles at  $-5^{\circ}\text{C}$  under a current density of  $0.1 \text{ A g}^{-1}$ , achieving a superior capacity of  $80 \text{ mAh g}^{-1}$ .<sup>[45]</sup>

Besides Al-based systems, a new eutectic electrolyte comprising  $\text{Zn}(\text{ClO}_4)_2 \cdot 6\text{H}_2\text{O}$ , ethylene glycol (EG), and  $\text{InCl}_3$  solution was developed for AZIBs, achieving an ESW of 3.3 V and a stable temperature range from  $-50$  to  $50^\circ\text{C}$ . Since eutectic system is governed by intermolecular interactions, adjusting molar ratios of individual components within the electrolyte is crucial for determining chemical properties such as ionic conductivity and thermal stability. Therefore, 0.1 M  $\text{InCl}_3$  was introduced as a cosolvent to enhance ionic conductivity of the hybrid electrolyte as shown in Figure 5g. In a similar fashion to other eutectic electrolytes, water molecules are confined through hydrogen bonding with EG and coordination with Zn ions. Additionally, by galvanic replacement ( $3\text{Zn} + 2\text{In}^{3+} \rightarrow 2\text{In} + 3\text{Zn}^{2+}$ ),  $\text{InCl}_3$  creates an *in situ* zincophilic In metal layer. As confirmed by XPS results, an SEI layer is formed, with a zincophobic top layer rich in Cl and a zincophilic bottom layer composed of In metal (Figure 5h). The resulting zincophilic/zincophobic bilayer interphase facilitates homogeneous Zn (002) deposition while preventing active water decomposition at the Zn electrode (Figure 5i). As a result, this electrolyte enables a high discharge capacity of  $82.7 \text{ mAh g}^{-1}$  in Zn/polyaniline (PANI) full cell over 2000 cycles under  $25^\circ\text{C}$ , at a current density of  $3 \text{ A g}^{-1}$ . This work elucidated the link between eutectic liquid network structure and electrode/electrolyte interphase chemistry with EG, non-toxic and biodegradable reagent.<sup>[46]</sup>

## 2.5. Cosolvents for Aqueous Electrolytes

Cosolvent strategy refers to the incorporation of organic compounds, such as polymers or organic solvents, that contain a high percentage of oxygen and nitrogen atoms into aqueous electrolytes. Similar to WIS electrolytes, cosolvents disrupt hydrogen bonding structure of water, significantly eliminating free water. However, cosolvent electrolytes are greener and more cost-effective than WIS electrolytes, as they need low salt concentrations, aided by the presence of cosolvent. In addition, although these electrolytes have low water percentage, they are mostly non-flammable, aligning with the development trend of minimizing water quantity while maintaining electrochemical performance.<sup>[22]</sup>

Su et al. developed water-in-sugar electrolyte by adding environmentally benign 5 M glucose into aqueous acids, realizing broad ESW of 3.9 V in proton batteries. This concentrated sugar cosolvent enters into hydronium solvation sheath and reduce the fraction of active water. Also, glucose preferentially adheres to the electrode and makes a film, contributing to its regulatory effect on water adsorption, as confirmed by transmission electron microscope (TEM) images (Figure 6a). Meanwhile, protons ( $\text{H}^+$ ), being the smallest and lightest ions, exhibit an exceptionally fast diffusion due to the Grotthuss mechanism, where protons transfer quickly through a hydrogen-bonded network of hydronium and water molecules, and the vehicle mechanism, where they diffuse as part of polyatomic ions, such as hydronium or ammonium. However, the simultaneous interaction of water and protons with electrode materials can

lead to structural deformation and reduced cycling stability. In contrast, adopting glucose cosolvent effectively inhibits water adsorption and desorption during proton intercalation and deintercalation. As a result,  $\text{MoO}_3$  anode with this cosolvent delivers stable cycling stability over 100000 cycles at  $30 \text{ A g}^{-1}$  with 72% capacity retention (Figure 6b).<sup>[47]</sup>

Furthermore, Li et al. utilized tetramethylurea (TMU), environmentally benign polar solvent, as a cosolvent for Zn aqueous battery. TMU strongly interacts with  $\text{Zn}^{2+}$  and water molecules through its C=O group, altering  $\text{Zn}^{2+}$  solvation structure and disrupting original hydrogen bonding in water. Also, due to the steric hindrance of  $-\text{N}(\text{CH}_3)_2$ , the primary  $\text{Zn}^{2+}$  solvation structure is protected from active  $\text{H}_2\text{O}$  molecules (Figure 6c). Hence, these factors help to reduce HER and Zn dendrite formation, inducing  $\text{Zn}/\text{NH}_4\text{V}_4\text{O}_{10}$  full cell to operate stably at  $0.5 \text{ A g}^{-1}$  for 300 cycles with a capacity retention of 68%, compared to only 3.9% without TMU as shown in Figure 6d.<sup>[48]</sup>

On the other hand, there is also a case where anode-free Zn metal batteries were achieved using a zinc triflate/propylene carbonate (PC)/water hybrid cosolvent electrolyte based on salting-in effect. Typically, practical AZIBs composed of thick Zn metal foil anodes ( $50$ – $200 \mu\text{m}$ ), which undermines overall energy density of cell. However, Ming et al. successfully developed anode-free Zn metal batteries with high energy density as illustrated in Figure 6e, using the cathode as sole source of  $\text{Zn}^{2+}$ , utilizing propylene carbonate as cosolvent. The hybrid cosolvent electrolyte enabled reversible  $\text{Zn}^{2+}$  deposition within current collector with high Coulombic efficiency (99.93% over 500 cycles at  $1 \text{ mA cm}^{-2}$ ), which is crucial for anode-free battery. Even at a low concentration of 2.14 M  $\text{Zn}(\text{OTf})_2$ , triflate anions were able to interfere  $\text{Zn}^{2+}$  solvation shell with assistance of PC cosolvent by forming the [PC-OTf-H<sub>2</sub>O] amphiphatic complex. This results in the creation of hydrophobic SEI layer, which decreases side reactions from water decomposition and suppresses the growth of Zn dendrites. Finally, stable anode-free Zn metal battery was achieved, demonstrating a promising cycling performance with 80% capacity retention after 275 cycles at  $0.5 \text{ mA cm}^{-2}$  (Figure 6f).<sup>[49]</sup>

Ether-based cosolvent electrolyte was also proposed by Miao et al., utilizing 1 m tetraglyme (G4),  $\text{Zn}(\text{OTf})_2$  salt, and water as synergistic hybrid cosolvent electrolyte for AZIBs, enhancing eco-friendliness by decreasing the required salt content. This cosolvent effectively prevents water-related side reactions by coordinating with Zn ion, forming hydrogen bonding with  $\text{H}_2\text{O}$  and preferentially adsorbing onto the Zn surface. This synergistic effect is amplified due to several O<sub>ether</sub> groups in the ether molecular framework of G4 (Figure 6g). As a result, PANI/carbon felt (CF) cathode employing this electrolyte retained 94% of its initial capacity after 1500 cycles at  $0.5 \text{ A g}^{-1}$ .<sup>[50]</sup>

Recently, Wang et al. employed isosorbide dimethyl ether (IDE) as a cosolvent for designing sustainable, biodegradable and non-flammable electrolytes for ALIBs (Figure 6h). This 1.85 m LiTFSI-H<sub>2</sub>O-IDE electrolyte (Figure 6i), with a molar ratio of 0.2:0.2:0.6, greatly increases ESW to 4.3 V and interferes with the Li ion solvation shell owing to the Li ion binding capability of IDE. Specifically, IDE constructs a five-membered ring

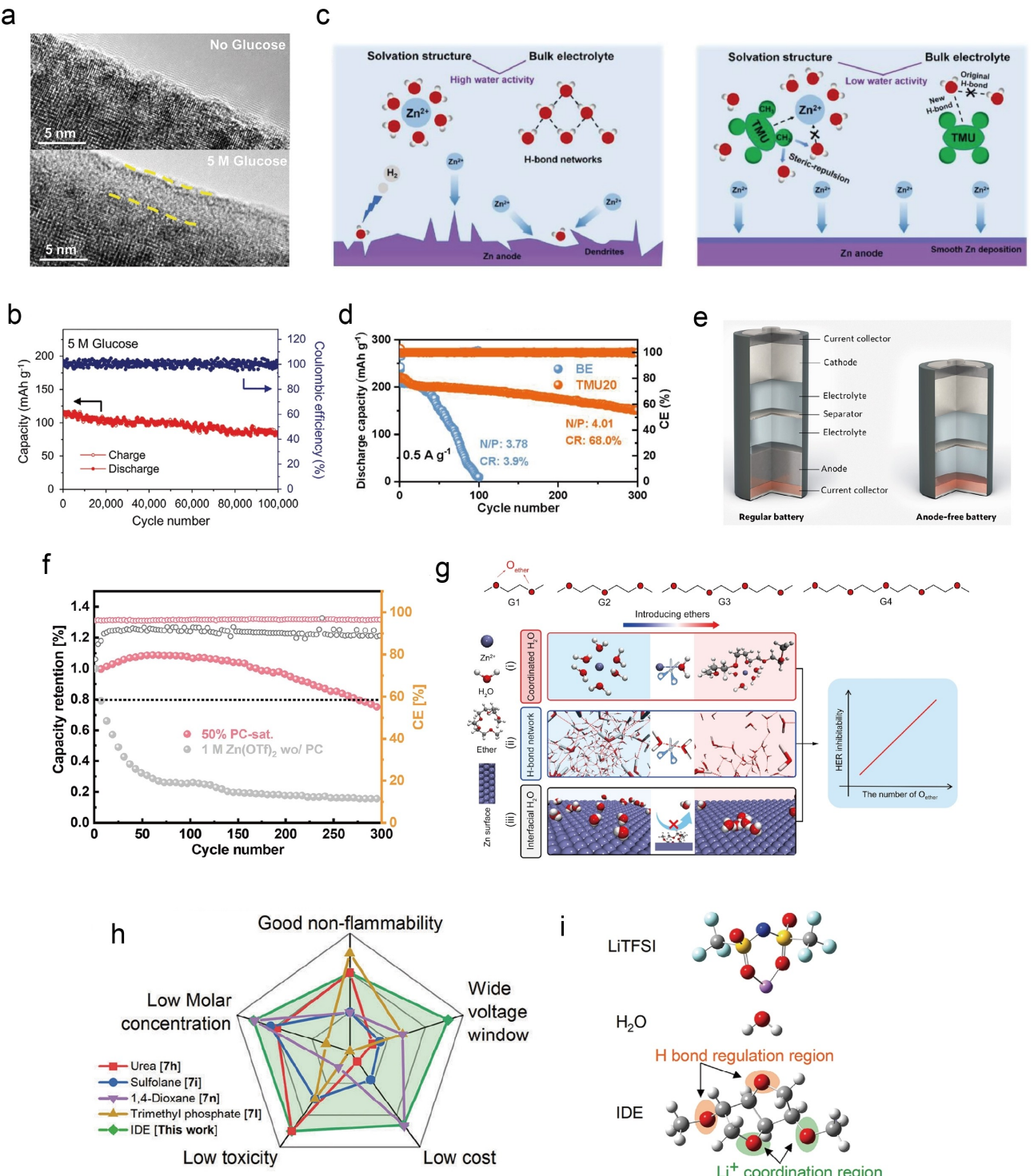


**Figure 6.** (a) TEM images of MoO<sub>3</sub> electrodes surface cycled with glucose-free and 5 M glucose electrolyte. Reproduced with permission.<sup>[47]</sup> Copyright 2021, Wiley-VCH. (c) Schematic illustration of Zn<sup>2+</sup> solvation structure in the 2 M Zn(OTf)<sub>2</sub>-H<sub>2</sub>O base electrolyte (BE) and with 20 vol% of TMU (TMU20). (d) Electrochemical performance of Zn/NH<sub>4</sub>V<sub>4</sub>O<sub>10</sub> full cell in the BE and TMU20 electrolyte at harsh conditions of 0.5 A g<sup>-1</sup>. Reproduced with permission.<sup>[48]</sup> Copyright 2023, Elsevier. (e) Configurations of typical Zn battery and anode-free Zn metal battery. (f) Electrochemical performance of anode-free Cu-ZnMn<sub>2</sub>O<sub>4</sub> batteries in several electrolytes at 0.5 mA cm<sup>-2</sup> ( $\approx$  350 mAh g<sup>-1</sup>). Reproduced with permission.<sup>[49]</sup> Copyright 2022, American Chemical Society. (g) Structures of four ether molecules with different O<sub>ether</sub> numbers (top) and three different functions of tetraglyme cosolvents (bottom). Reproduced with permission.<sup>[50]</sup> Copyright 2022, Elsevier. (h) Radar plots for several cosolvents in aqueous electrolytes. (i) Chemical structure of LiTFSI, H<sub>2</sub>O, IDE. Reproduced with permission.<sup>[51]</sup> Copyright 2024, Wiley-VCH.

structure through oxygen atoms of the endo-OCH<sub>3</sub> and the opposite cyclic ether within the same plane. Additionally, IDE effectively suppresses HER due to its steric hindrance effect, which arises from its unique 3D asymmetric bicyclic molecular structure with two non-planar rings. This structure weakens its Li<sup>+</sup> solvation ability and induces more anions to join the primary Li<sup>+</sup> solvation sheath, resulting in the formation of multiple ion pairs. Consequently, a durable SEI layer is formed, enriched with both fluoride-rich components and flexible organics. With this electrolyte, a stable Li<sub>4</sub>Ti<sub>5</sub>O<sub>12</sub>(LTO)/LiMn<sub>2</sub>O<sub>4</sub> (LMO) full cell was realized, which delivered an average Coulombic efficiency of 99.35% over 450 cycles at 2 C.<sup>[51]</sup>

### 3. Sustainable Electrolytes for Subzero Applications

Beyond advancing greener technology, the current climate situation with extreme temperature variations caused by global warming demands new strategies for sustainable living.<sup>[52]</sup> While most research so far has focused on performance at room-temperature, it is also crucial to investigate the behavior of metal ion deposition and stripping at extreme temperatures. However, the aforementioned high-voltage electrolytes, exhibit increased viscosity and decreased solubility as temperatures drop.<sup>[53]</sup> This makes it challenging to operate aqueous batteries efficiently under extreme temperature conditions. Therefore, addressing the issue of poor low-temperature performance in aqueous batteries is essential for establishing reliable energy storage systems capable of withstanding a rapidly changing climate.

At low-temperatures, aqueous electrolytes face several challenges that must be managed to ensure optimal performance of AIBs. A primary issue is the formation of strong hydrogen bonds that occur during the phase transition from water into ice.<sup>[54]</sup> This transition leads to a significant decrease in conductivity and reduces the wettability of the solution.<sup>[55]</sup> Additionally, the viscosity of the electrolyte increases, which can impede ion mobility and thus slow down the charge transfer processes. As the phase transition proceeds, it also undergoes volume expansion, which can cause detachment between the electrolyte and the electrode. This separation hinders efficient electrochemical reactions, further degrading battery performance.<sup>[54]</sup> Managing these factors is crucial because they collectively impact the overall efficiency and reversibility of AIBs under freezing temperatures. Consequently, various studies have been reported to improve battery performance at low-temperatures. However, the use of harmful organic salts or solvents is sometimes unavoidable to improve low-temperature performance. Ideally, minimizing the use of these toxic substances is necessary to develop sustainable batteries. Therefore, we aim to introduce research that has achieved electrolyte optimization for low-temperature operation using non-toxic materials, categorized into four major strategies: (1) hydrogel electrolytes, (2) additives and cosolvents, (3) WIS electrolytes, and (4) eutectic electrolytes.

#### 3.1. Hydrogel Electrolytes

Hydrogels are mainly composed of cross-linked polymer chains and have properties that can vary depending on the functional groups, allowing for the adjustment of anti-freezing effects.<sup>[56]</sup> In this case, the strong interaction between the hydrogel and water helps to alleviate the sluggish ion movement caused by the strengthened hydrogen bonds at low-temperatures.<sup>[57]</sup> Quasi-solid electrolytes, such as hydrogels, have characteristics that can overcome various limitations of liquid electrolytes using water as a solvent. The significantly reduced amount of water decreases the occurrence of side reactions caused by water, while the elasticity and high strength provide a robust protective layer inside the battery. However, since they still contain water, they tend to freeze at subzero temperatures, and various studies have been reported to address this issue.

The polymers commonly used in hydrogels are polyacrylamide (PAM) and poly(vinyl alcohol) (PVA). An example of a PAM-based hydrogel for AZIBs includes PAM hydrogel electrolytes with 2 M ZnSO<sub>4</sub> and 4 M LiCl (ZL-PAAm). Before discussing anti-freezing effects, it is important to prevent side reactions such as the chronic HER in AZIBs. To achieve this, a commonly used strategy is the suppression of Zn ion hydration. However, hydration is necessary to lower the freezing point, creating a conflicting issue. Therefore, O. G. Schmidt's group induced cooperative hydration using two types of salts, ZnSO<sub>4</sub> and LiCl, and demonstrated excellent anti-freezing effects by reducing the intramolecular hydrogen bonds in the framework through the use of a mixture of these two types of cations (Figure 7a, b). In addition, they significantly reduced the formation of by-products such as Zn(OH)<sub>2</sub> and ZnO by suppressing HER. Consequently, a Zn/LiFePO<sub>4</sub> hybrid full cell showed about 98% capacity retention for 500 cycles at -20°C (Figure 7c).<sup>[58]</sup> Another example includes AZIBs using PAM, Zn(CF<sub>3</sub>SO<sub>3</sub>)<sub>2</sub>, and Gly. Gly is widely known for its anti-freezing and anti-drying effects. Thus, R. Wang et al. constructed a 3D porous PAM matrix with Gly. The abundant hydroxyl groups of Gly, existing between PAM chains, weakened the strong hydrogen bonds between water molecules. Density functional theory (DFT) calculations demonstrated that the Gly-H<sub>2</sub>O interaction is much stronger than the H<sub>2</sub>O-H<sub>2</sub>O interaction. The resulting gel electrolyte not only lowered the freezing point but also showed anti-drying effects, achieving a Zn/PANI full cell with 76.8% capacity retention at -40°C.<sup>[60]</sup>

Various studies have utilized PAM and DMSO together. DMSO promotes stable Zn deposition and forms strong hydrogen bonds with water molecules, organizing the structure within the electrolyte, making it useful not only for hydrogels but also for various types of aqueous electrolytes. H. Lu et al. developed a hydrogel electrolyte using PAM, DMSO, and Zn(CF<sub>3</sub>SO<sub>3</sub>)<sub>2</sub> (PDZ-H). DMSO undergoes reductive decomposition in the electrolyte, forming a SEI layer on the Zn anode, promoting uniform Zn deposition (Figure 7d). The synergistic effects of PAM's strengths in low-temperature environments and DMSO's dendrite suppression effects led to the demonstration of a Zn<sub>3</sub>V<sub>2</sub>O<sub>8</sub>/Zn/PDZ-H full cell operating at low-temperatures (Figure 7e).<sup>[59]</sup> According to the US Environmental

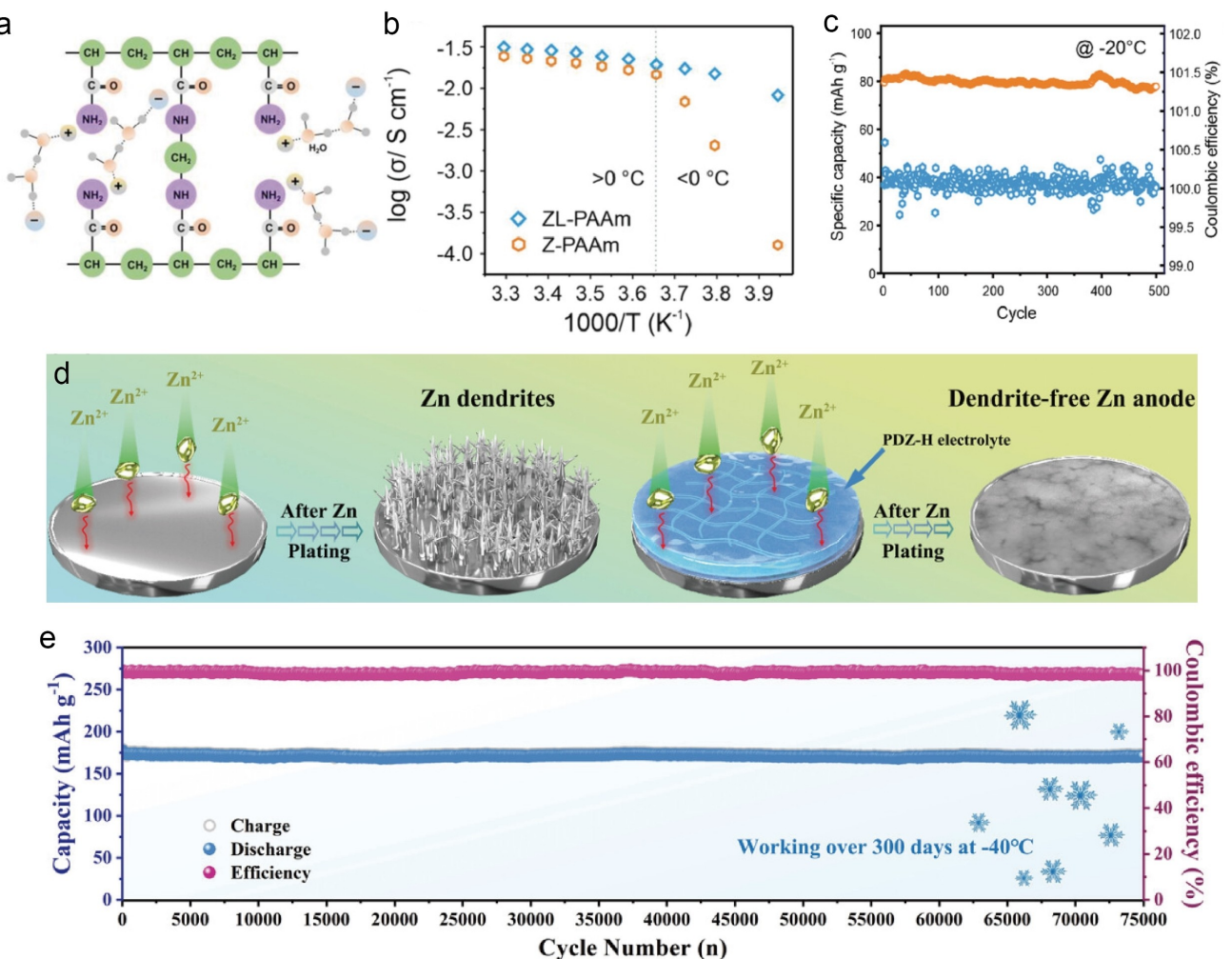


**Figure 7.** a) Schematic illustration of chemical structure of ZL-PAAm. b) Ionic conductivities of ZL-PAAm and Z-PAAm at different temperatures. c) Cycle performance of Zn/LiFePO<sub>4</sub> battery based on ZL-PAAm at -20 °C. Reproduced with permission.<sup>[58]</sup> Copyright 2019, Wiley-VCH. d) Schematic illustration of Zn deposition morphology of Zn/Z-AE and Zn/PDZ-H. e) Cycling stability of Zn<sub>3</sub>V<sub>2</sub>O<sub>8</sub>/Zn/PDZ-H cell at -40 °C. Reproduced with permission.<sup>[59]</sup> Copyright 2022, Wiley-VCH.

Protection Agency (EPA), DMSO is classified as a nontoxic solvent, gaining attention as a green solvent in organic synthesis.<sup>[61]</sup> However, salts such as Zn(CF<sub>3</sub>SO<sub>3</sub>)<sub>2</sub> are primarily used, and their high fluorine content can be a major cause of pollution. Therefore, to ultimately achieve environmentally friendly batteries, it is necessary to combine hydrogel with eco-friendly salts like ZnSO<sub>4</sub> to maintain excellent performance even at low-temperatures.

X. Hou's group developed a hydrogel electrolyte using PAM, cellulose nanofibers (CNF), and DMSO, employing 2 M ZnSO<sub>4</sub> and 0.2 M MnSO<sub>4</sub> as electrolyte salts (Figure 8a). Acting as a hydrogen bond acceptor, DMSO formed strong hydrogen bonds, enhancing the mechanical strength of the hydrogel and significantly lowering the freezing point. Additionally, the well-known dendrite suppression effect of DMSO realized a Zn/MnO<sub>2</sub>/CNT full cell operating from room temperature to -20 °C (Figure 8b).<sup>[62]</sup> Another excellent example of an eco-friendly hydrogel electrolyte, inspired by epidermal tissue, is the EG-based Zn-alginate/PAM organohydrogel (BM-gel) reported by

C. Zhi's group (Figure 8c). According to the NTIS's public health statement, EG is biodegradable within days to weeks in marine or soil environments and is widely used as a green material due to its nontoxic anti-freezing effect.<sup>[63]</sup> In this study, EG and water molecules formed a matrix, creating strong hydrogen bond, which effectively prevented water crystallization at low-temperatures, lowering the freezing point to -23 °C and resulting in high ionic conductivity of 14.1 mS/cm at -20 °C (Figure 8d). Using the BM-gel with excellent anti-freezing and water retention effects, they achieved a stable Zn/MnO<sub>2</sub> battery operating in a wide temperature window (-20 to 80 °C) (Figure 8e).<sup>[63]</sup> Another study using EG and ZnSO<sub>4</sub> reported that, in addition to the anti-freezing agent, it also functions as a non-flammable aqueous electrolyte.<sup>[66]</sup> M. Chen et al. extracted cellulose from cotton, which is biodegradable natural fabric, and formed a polymeric framework with tetraethyl orthosilicate (TEOS) and Gly, demonstrating that the abundant hydroxyl groups prevented the crystallization of water molecules (Figure 8f, g). Furthermore, the addition of ZnSO<sub>4</sub> and MnSO<sub>4</sub>

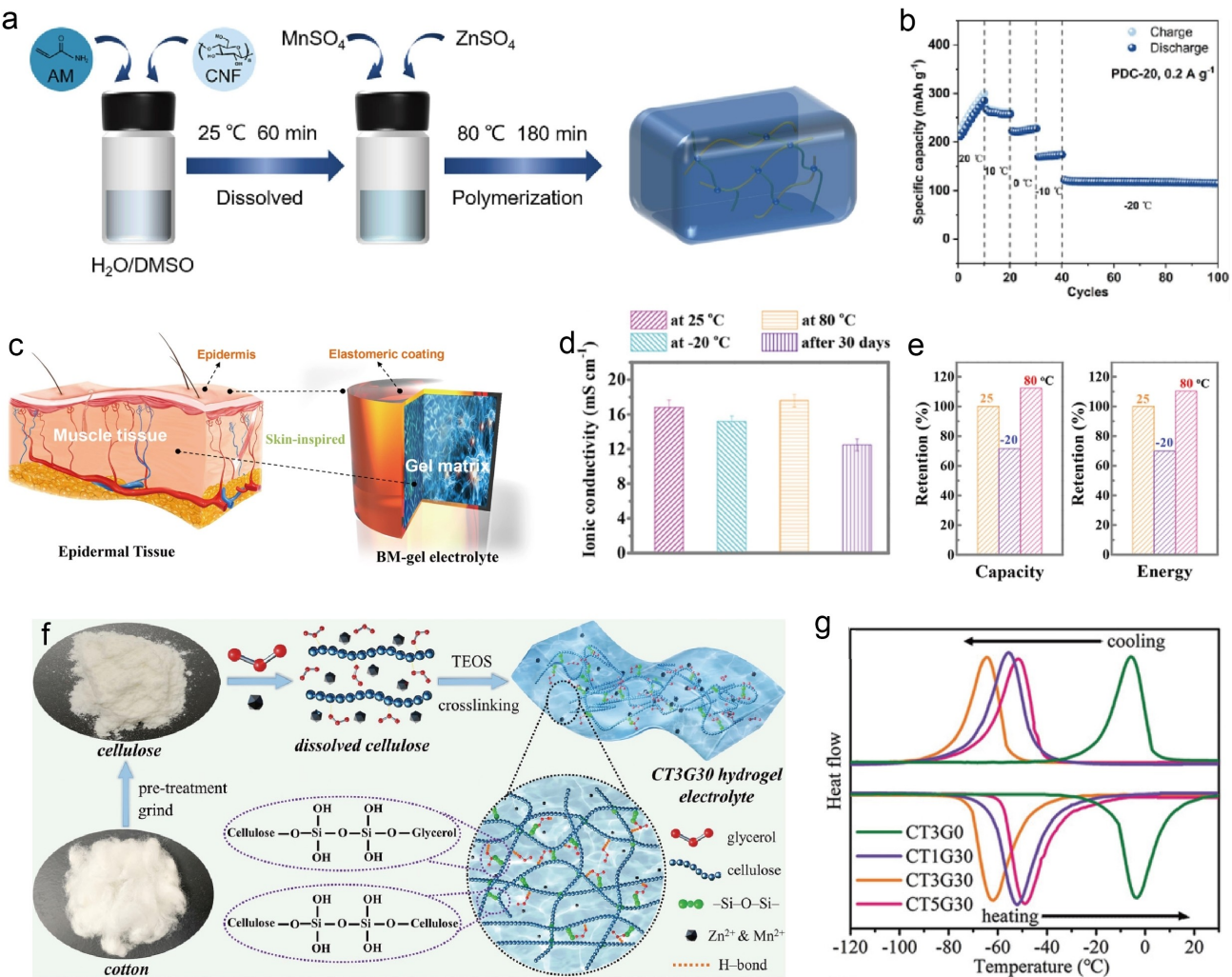


**Figure 8.** a) Schematic illustration of PDC-20 preparation. b) Electrochemical performance of Zn/MnO<sub>2</sub>/CNT full cell with PDC-20 from 20 °C to -20 °C. Reproduced with permission.<sup>[62]</sup> Copyright 2023, Elsevier. c) Scheme of skin-inspired BM-gel design. d) Ionic conductivities of the BM-gel electrolytes at various temperatures. e) Capacity retentions and energy density of Zn-MnO<sub>2</sub> battery using BM-gel electrolyte at different temperatures. Reproduced with permission.<sup>[63]</sup> Copyright 2019, Wiley-VCH. f) Schematic illustration of CT3G30 hydrogel synthesis. g) DSC curves of CT3G0, CT1G30, CT3G30, and CT5G30. Reproduced with permission.<sup>[64]</sup> Copyright 2021, Wiley-VCH.

further enhanced the anti-freezing effect, achieving excellent battery performance with 83.8% capacity retention over 2000 cycles at -40 °C.<sup>[64,67]</sup>

### 3.2. Additives and Cosolvents for Aqueous Electrolytes

Additives or cosolvents are well-known strategies for optimizing the electrolyte by mixing relatively small amounts of substances into it. Recently, many studies have reported improving low-temperature performance by mixing organic solvents to create so-called "aqueous/nonaqueous hybrid electrolytes".<sup>[68]</sup> From an environmental perspective, the advantage of using additives or cosolvents is that they have a relatively lower environmental impact and cost burden, due to the small amounts of substances used compared to other types of electrolytes. J. Chen's group demonstrated how the chaotropic anion, CF<sub>3</sub>SO<sub>3</sub><sup>-</sup>, creates

-34.1 °C suitable environment for low-temperature AIIBs. The most negative electrostatic potential (ESP) was proposed as a key factor in revealing the correlation between various anions (SO<sub>4</sub><sup>2-</sup>, NO<sub>3</sub><sup>-</sup>, Cl<sup>-</sup>, I<sup>-</sup>, and CF<sub>3</sub>SO<sub>3</sub><sup>-</sup>) in water at subzero temperatures. The higher the most negative ESP of an anion, the weaker the interaction between H<sub>2</sub>O/Zn<sup>2+</sup> and the anion. By DFT calculation, CF<sub>3</sub>SO<sub>3</sub><sup>-</sup> was identified as having the highest ESP. MD simulation showed that the Zn<sup>2+</sup>-water coordination number and hydrogen bond number had a strong correlation with the most negative ESP. Due to the low H<sub>2</sub>O/Zn<sup>2+</sup> binding energy of CF<sub>3</sub>SO<sub>3</sub><sup>-</sup>, the number of hydrogen bonds decreased, and the ratio of relatively weak hydrogen bonds increased, which could explain the decrease in the electrolyte's freezing point (Figure 9a). Based on these results, using a 2 M Zn-(CF<sub>3</sub>SO<sub>3</sub>)<sub>2</sub> aqueous solution, a Zn/V<sub>2</sub>O<sub>5</sub> full cell showed a capacity of 285 mAh g<sup>-1</sup> at -30 °C and operated stably for over 1000 cycles.<sup>[69]</sup> There has also been research where 20 vol% of PC was added as a cosolvent to a 3 M Zn(CF<sub>3</sub>SO<sub>3</sub>)<sub>2</sub> electrolyte,

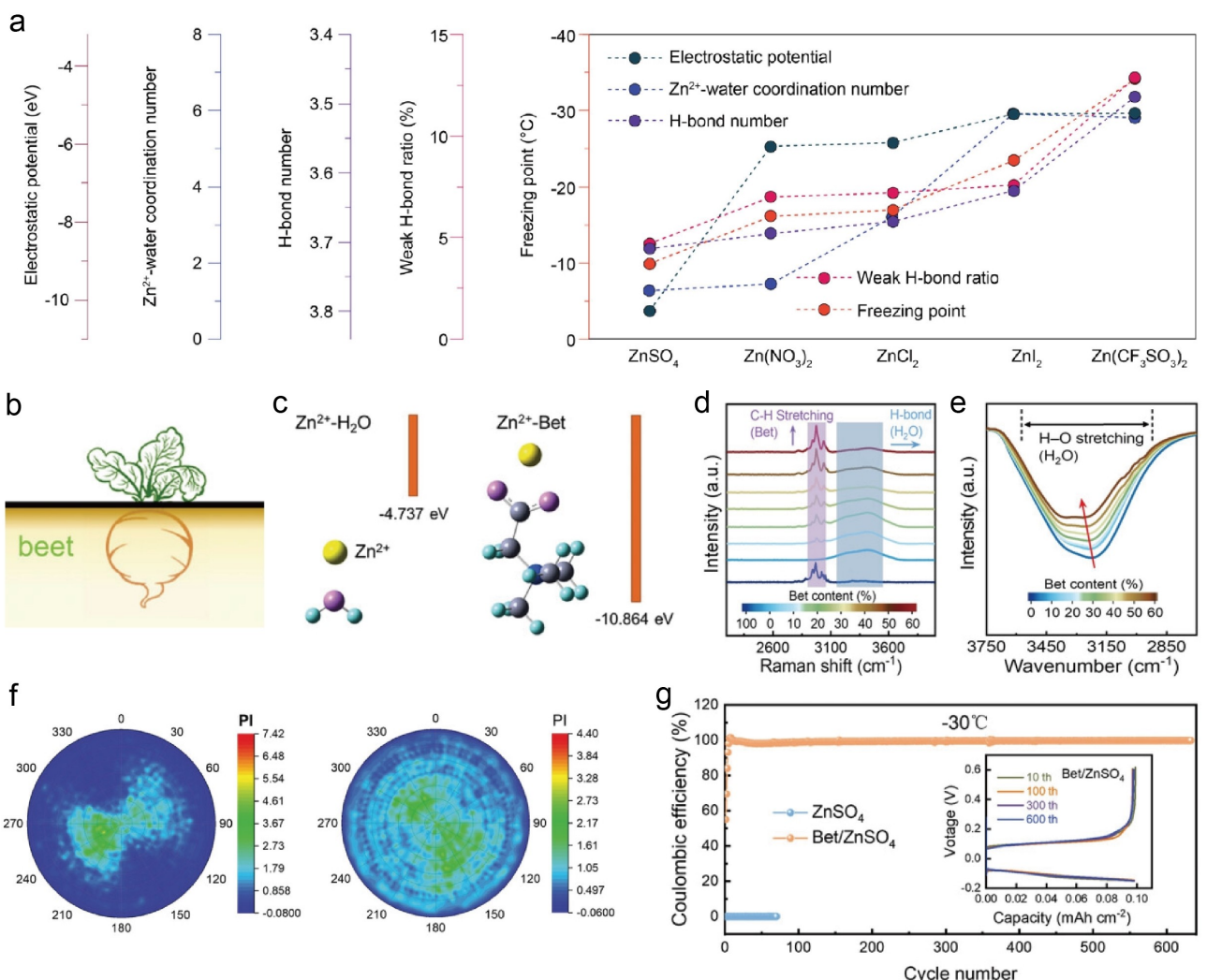


**Figure 9.** a) Correlations between various characteristics of different electrolytes. Schematic illustration of PDC-20 preparation. Reproduced with permission.<sup>[69]</sup>. Copyright 2021, American Chemical Society. b) Scheme of beet, which is the source of Bet. c) Binding energy of  $Zn^{2+}$ - $H_2O$  and  $Zn^{2+}$ -Bet. d) Raman spectra of Bet/ $ZnSO_4$  electrolyte with different Bet contents. e) ATR-FTIR spectra of Bet/ $ZnSO_4$  with different Bet contents. f) XRD pole figures of Zn anodes after 50 cycles in blank  $ZnSO_4$  and Bet/ $ZnSO_4$  electrolyte. g) Cycling stability of Zn/ $V_2O_5$  full cell with Bet/ $ZnSO_4$  electrolyte at  $-30^{\circ}C$ . Reproduced with permission.<sup>[74]</sup>. Copyright 2022, Wiley-VCH.

dramatically lowering the electrolyte's freezing point to  $-69^{\circ}C$ .<sup>[70]</sup>

However, from an environmental perspective, as mentioned earlier, there are some drawbacks to using this salt as the main electrolyte component. Therefore, greater emphasis is placed on this review on improving low-temperature performance using environmentally friendly and naturally available materials. The anti-freezing effect of the green solvent DMSO has already been reported in several hydrogel electrolyte studies, and DMSO showed a similar effect when used as an electrolyte additive.<sup>[41]</sup> EG is widely used not only as a hydrogel electrolyte but also as a cosolvent for aqueous electrolytes to realize stable batteries in low-temperature environments.<sup>[71]</sup> Another good example of eco-friendly ALBs is a study using 1,3-propanediol (PG), which can be extracted from corn and is biodegradable.<sup>[72]</sup> PG, with its high donor number, can easily interact with  $Zn^{2+}$  and has been shown to weaken hydrogen bonds. This allowed

the electrolyte's freezing point to be lowered to  $-35^{\circ}C$ , demonstrating  $Zn/V_2O_5$  batteries to operate at  $-20^{\circ}C$ .<sup>[73]</sup> Another example of an environmentally friendly additive suitable for low-temperatures is betaine (Bet), a nontoxic biological osmolyte extracted from beet plants. H. Ren et al. utilized Bet by mixing it into 1 M  $ZnSO_4$  as a remarkable anti-freezing additive. Bet interacted more strongly with Zn ions than with water molecules, altering the solvation structure of Zn ions (Figure 9b). Similar to the previous anti-freezing additives, Bet interacted more strongly with Zn ions than with water molecules, altering the solvation structure of Zn ions (Figure 9c). Raman spectroscopy revealed that as Bet content increased, the interaction between Bet and water molecules strengthened, and attenuated total reflection Fourier transform infrared (ATR-FTIR) confirmed that Bet weakened the interactions between water molecules (Figure 9d, e). As shown by the XRD pole figures, Bet additives induced the Zn deposition in orientation of the (002) plane, resulting in a much more uniform Zn deposition morphology (Figure 9f). Additionally, the effects

of suppressing HER and corrosion were also confirmed. As a result, they succeeded in lowering the electrolyte's freezing point to as low as  $-92^{\circ}\text{C}$ , and reported Zn/VO<sub>2</sub> batteries operating at  $-30^{\circ}\text{C}$  (Figure 9g).<sup>[74]</sup>

### 3.3. Water-in-Salt Electrolytes

WIS electrolytes have a wide ESW and are being researched in various ways for high performance ALBs. However, in WISs, the amount of water must be extremely limited and the salt concentration increased to achieve the anti-freezing effect, making the inherent properties of the salt critical to battery performance. Typically, WIS electrolytes use a significant amount of salt, which already reaches nearly the maximum solubility at room temperature, and when the temperature drops, a rapid water-ice phase transition can easily occur. Therefore, there are relatively few studies that have achieved WIS electrolytes at subzero temperatures compatibility. In addition, it is particularly difficult to develop electrolytes made of environmentally friendly materials among them, so while introducing traditional WIS electrolytes, we aim to provide a direction for sustainable WIS electrolytes.

As mentioned above, the concept of WIS electrolyte was first introduced by reporting 21 m LiTFSI electrolyte for high-voltage ALBs.<sup>[20]</sup> The C. Battaglia group reported that asymmetric anions, such as FTFSI<sup>-</sup>, suppress the crystallization of WIS electrolytes at low-temperatures.<sup>[75]</sup> In this study, one of the previously introduced WIS electrolytes, 35 m sodium bis(fluorosulfonyl)imide (NaFSI), was partially replaced with sodium (fluorosulfonyl)(trifluoromethylsulfonyl)imide (NaFTFSI) containing asymmetric anions, and it was confirmed that crystallization does not occur even when it was operated near the salt solubility limit at room temperature. Crystallization suppression is also observed in Li-based systems. At  $0^{\circ}\text{C}$ , when an asymmetric 10 m LiTFSI anion is mixed, the electrolyte remains in the liquid state for a longer time compared to other WIS electrolytes with mixed symmetric anions (Figure 10a). Therefore, this study demonstrated that asymmetric anions play a role in preventing the crystallization of aqueous electrolytes, and other asymmetric anions for WIS electrolytes to suppress ice crystallization have been widely reported. A representative example is the (pentafluoroethanesulfonyl)(trifluoromethane-sulfonyl)imide (PTFSI) anion, which claims that LiPTFSI has a relatively stable structure compared to other anions because it lacks an S–F bond (Figure 10b). As confirmed by the DSC curves, LiPTFSI shows the lowest liquidus temperature among LiTFSI, LiOTf, and LiPTFSI, and the electrolyte mixed with LiPTFSI and LiOTf in a 15:5 ratio exhibited an even lower liquidus temperature (Figure 10c). Although the liquidus temperature is lowest at 10 m LiPTFSI, it was reported that an appropriate mixing ratio was chosen to maximize the wide ESW, which is a critical advantage of WIS electrolytes (Figure 10d).<sup>[76]</sup>

The ClO<sub>4</sub> anion is another representative material used for WIS electrolytes. There is research where ANIBs operating at  $-40^{\circ}\text{C}$  were implemented using a flexible microelectrode and 17 m NaClO<sub>4</sub> WIS electrolyte.<sup>[77]</sup> Recently, a micelle-like structure

WIS electrolyte was reported using cosolvent with low donor number and amphiphilic anion. In particular, the ternary interaction between salt, water, and organic cosolvent was analyzed at both the atomic and macroscopic scales. The electrostatic interactions between salt and water or organic cosolvent, as well as hydrogen bonding and van der Waals forces between water and organic cosolvent, determine the solvation structure of the cations (Figure 10e). To form the micelle-like structure, organic cosolvents with intermediately low donor numbers, such as acetonitrile (ACN) and 1,3-Dioxolane (DOL), were required, and amphiphilic, low polarity anions, such as OTf anion, were determined as suitable salts. The electrolyte with the most outstanding anti-freezing effect was the micelle-like electrolyte with Zn(OTf)<sub>2</sub> in DOL/H<sub>2</sub>O with a molar ratio of 1:1 (MSE-1D1 W), and using cryogenic in situ optical microscopy, it was demonstrated that this electrolyte remained in a liquid state down to  $-96^{\circ}\text{C}$  (Figure 10f). In the benchmark electrolyte (BE) with 1 M Zn(OTf)<sub>2</sub> aqueous solution, the strong hydrogen bonds between water molecules, causing a rapid water-ice transition at subzero temperatures, hindered the movement of Zn ions. In contrast, in MSE-1D1 W, the anion reduced the ratio of strong hydrogen bonds and changed the solvation structure of Zn ions, showing an effect of suppressing ice crystallization (Figure 10g). Furthermore, it was demonstrated that up to 29.8 m of Zn(OTf)<sub>2</sub> could dissolve within this micelle-like structure, and based on the aforementioned effects, a Zn/PANI cell operating at  $-80^{\circ}\text{C}$  for 5000 cycles was achieved (Figure 10h).<sup>[78]</sup> Although the effects of Zn(OTf)<sub>2</sub> on human health and the environment are controversial, DOL, the cosolvent used to increase the solubility of the salt, is non-toxic and non-carcinogenic.<sup>[72]</sup> Compared to other electrolytes, this approach may not yet be very environmentally friendly. However, as highlighted in the research above, replacing even one component with a green material may currently be the most effective way to improve the environmental sustainability of aqueous electrolytes. Furthermore, given the challenges of completely replacing hazardous salts due to solubility and ionic conductivity concerns, maximizing salt reuse through recycling technologies may be a practical solution.<sup>[79]</sup>

### 3.4. Eutectic Electrolytes

Eutectic electrolytes are those that utilize the theory of achieving phase equilibrium with water, the solvent, at the lowest eutectic point according to the water-salt phase diagram. This significantly lowers the freezing point and improves the anti-freezing effect of the electrolytes.<sup>[80]</sup> Due to the chemical properties of these eutectic electrolytes, they possess a much lower solid-liquid transition temperature than other electrolytes, resulting in superior performance at extremely low-temperatures. Although their low-temperature adaptability is relatively superior, eutectic electrolytes primarily require chloride- or fluoride-based salts, and to form a eutectic compound, harmful chemicals such as succinonitrile (SN) and sulfolane (SL) are used to improve low temperature performance.<sup>[83]</sup> A representative chloride-based salt is ZnCl<sub>2</sub>,

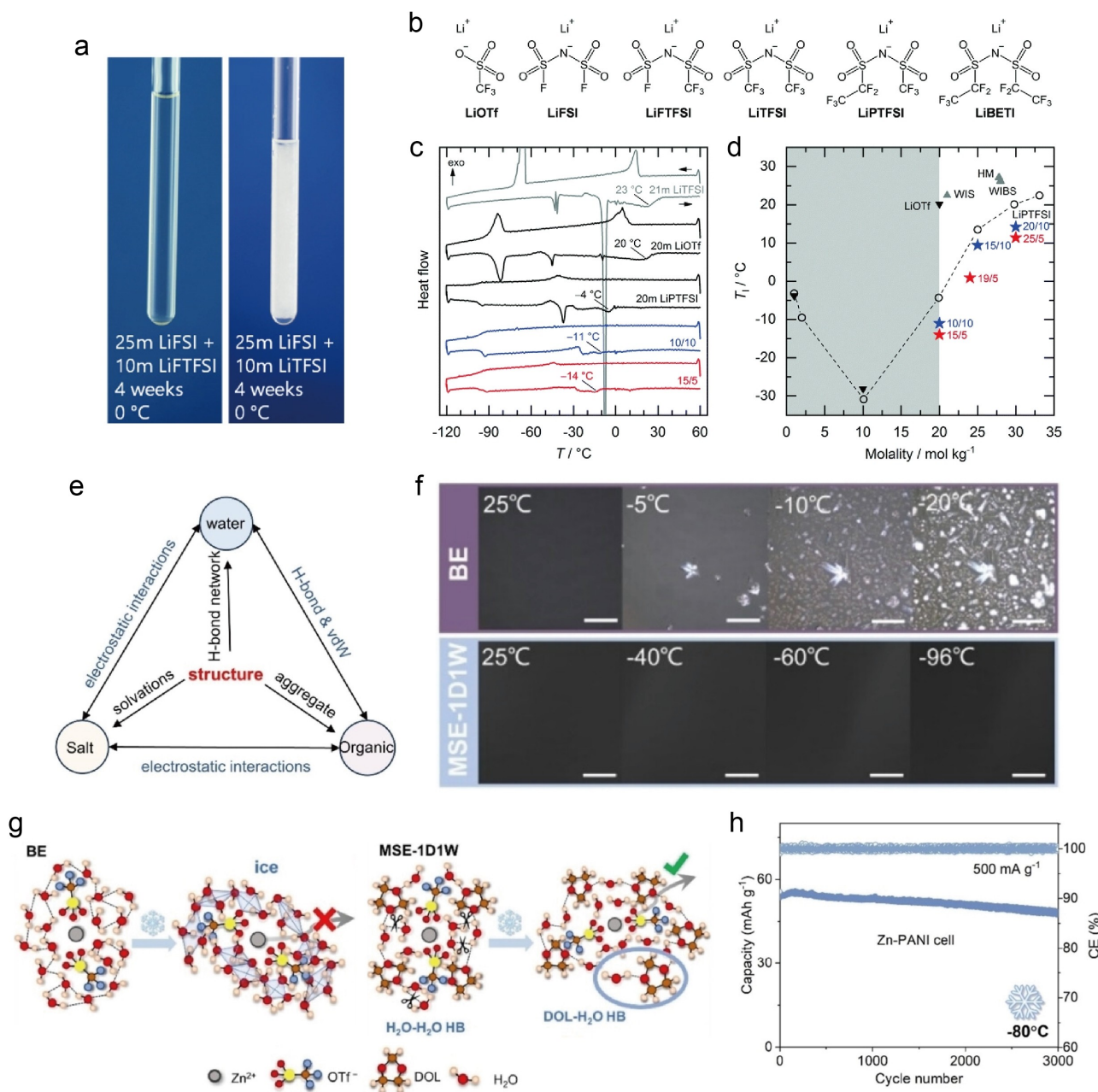


**Figure 10.** a) Photographs of 25 m LiFSI + 10 m LiFTFSI and 25 m LiFSI + 10 m LiTFSI electrolytes stored at 0 °C for 4 weeks. Reproduced with permission.<sup>[75]</sup> Copyright 2019, American Chemical Society. b) Chemical structures of LiOTf and sulfonylimide-based Li salts. c) DSC curves of different electrolytes with approximately 20 m salt concentrations. d) Liquidus temperature of different electrolytes. Reproduced with permission.<sup>[76]</sup> Copyright 2019, Royal Society of Chemistry. e) The correlations and interactions of electrolyte compositions. f) In situ optical microscopy images of the freezing process of BE and MSE-1D1 W. g) Schematic illustration of the structural evolution of BE and MSE-1D1 W at subzero temperature. h) Cycling stability of Zn/PANI cell with MSE-1D1 W at -80 °C. Reproduced with permission.<sup>[78]</sup> Copyright 2024, Wiley-VCH.

which has been reported to lower the freezing point to an extreme low -114 °C using 7.5 m ZnCl<sub>2</sub>.<sup>[81]</sup> Through various spectroscopic characterizations and MD simulations, it was found that ZnCl<sub>2</sub> achieves this effect by weakening the strong hydrogen bonds of water molecules (Figure 11a). A Zn/PANI full cell with 7.5 m ZnCl<sub>2</sub> eutectic electrolyte operated stably from room temperature down to -50 °C (Figures 11b, c). In addition, it showed nearly 100% capacity retention over 2000 cycles in an extremely cold environment of -70 °C. Moreover, in a pouch

cell with stacked electrodes, it showed ≈43.4% of its capacity compared to room temperature (Figures 11d, e). Additionally, some studies have reported that the addition of SnCl<sub>2</sub> to ZnCl<sub>2</sub> improves the low-temperature performance, further demonstrating the effect of ZnCl<sub>2</sub> in various aspects.<sup>[84]</sup> However, as reported in several studies, chloride ions are corrosive, toxic, and harmful to the environment and humans when released into nature, which requires their long-term replacement with green materials.<sup>[85]</sup>

**Table 1.** Electrochemical performance of batteries with aqueous electrolyte at low-temperatures.

Type of electrolytes	Electrolyte	Ionic conductivity [mS cm <sup>-1</sup> ]	Freezing point [°C]	Operating temperature range [°C]	Anode	Cathode	Initial capacity [mAh g <sup>-1</sup> @A g <sup>-1</sup> ]	Cycles	Retention [%]	Temperature [°C]	Ref.
Hydrogel electrolyte	Gly-H <sub>2</sub> O (2:1 wt%)	8/RT	<-80	-10–25	Ni <sub>2</sub> ZnHCF	PTCDI	40@0.1	100	—	-10	[87]
	1 M Li <sub>2</sub> SO <sub>4</sub> + EtG (40 wt%)	≈4.2/-20	-24.6	-20–0	Li	LiFePO <sub>4</sub>	≈93@0.085	100	—	-20	[88]
	PDC-20	1.52/-30	<-40	-20–20	Zn	MnO <sub>2</sub> /CNT	118@0.2	350	61.5	-20	[62]
	ZL-PAAm	≈17/-20	-45	-20–25	Zn	LiFePO <sub>4</sub>	≈80@0.5	500	98	-20	[58]
	BM gel	14.1/-20	-23	-20–80	Zn	MnO <sub>2</sub>	115.2@1.6	500	66	-20	[63]
	CSAM-C	7.8/-30	<-31	-30–25	Zn	PANI	≈75@5	2500	—	-30	[89]
	EG@0.2 M MnSO <sub>4</sub> + 2 M ZnSO <sub>4</sub>	13.32/RT	<-30	-30–30	Zn	MVO	23.1.13@0.2	1000	85	-30	[71]
Hydrogel electrolyte	PVA/G	10.7/-30	—	-30–60	Zn	δ-Mg <sub>2</sub> O	174.5@2	5000	87.7	-30	[90]
	OHE	1.62/-30	<-60	-30–80	Zn	PANI	≈105@0.2	1500	88.8	-30	[91]
	PVA-B-G	10.1/-35	<-60	-35–25	Zn	MnO <sub>2</sub>	≈125@1	2000	89.4	-35	[92]
	PAM-H <sub>2</sub> O-Gly 20%	0.097/-40	<-40	-40–20	Zn	SWCNTs/PANI	≈50@1	500	76.8	-40	[60]
	PAAm/DMSO/Zn-(CF <sub>3</sub> SO <sub>2</sub> ) <sub>2</sub>	≈3/-20	—	-40–60	Zn	Zn <sub>3</sub> V <sub>2</sub> O <sub>8</sub>	≈175@2	75000	—	-40	[59]
	ZnSO <sub>4</sub> /H <sub>2</sub> O + 50 % EG	≈7/RT	-43.2	-40–60	Zn	PQ-MCT	≈60@0.2	8000	—	25	[66]
	CT3G30	19.4/-40	-64.6	-40–60	Zn	MnO <sub>2</sub>	≈137@3	2000	83.8	-40	[64]
	2 M ZnSO <sub>4</sub> + 20 vol % DMSO	2/-20	-34.51	-20–20	Zn	MnO <sub>2</sub>	≈100@1 C	300	—	-20	[41]
	3 M ZnSO <sub>4</sub> + 20 vol % PG	—	-35	-20–25	Zn	V <sub>2</sub> O <sub>5</sub>	190@0.5	500	—	-20	[73]
	12SL-4H <sub>2</sub> O-3LiClO <sub>4</sub>	0.12/-40	-110	-20–25	Zn	Li <sub>4</sub> Ti <sub>5</sub> O <sub>12</sub>	≈48@0.2	200	87	-20	[93]
	2 M Zn(CF <sub>3</sub> SO <sub>2</sub> ) <sub>2</sub>	4.47/-30	-34.1	-30–25	Zn	V <sub>2</sub> O <sub>5</sub>	194.1@1	1000	81.7	-30	[69]
	3 M Zn(OTf) <sub>2</sub> + 1 wt % APA	—	—	-30–50	Zn	NVO	180@5	3650	86.8	25	[94]
Additive/co-solvents	Bet/ZnO <sub>4</sub>	0.935/-35	-92	-30–60	Zn	VO <sub>2</sub>	61.25@2	160	—	-30	[74]
	2 M ZnSO <sub>4</sub> + 60 vol % EG	6.9/-40	-33	-40–20	Zn	PANI-V <sub>2</sub> O <sub>5</sub>	100@0.2	250	—	-20	[95]
	3 M Zn(CF <sub>3</sub> SO <sub>2</sub> ) <sub>2</sub> + 20 vol% PC	3.75/-40	-69	-40–25	Zn	NVO	168@0.2	400	100	-40	[70]
	3 M Zn(ClO <sub>4</sub> ) <sub>2</sub>	4.23/-50	-74	-50–25	Zn	a-MnO <sub>2</sub>	≈40@6	1000	—	-50	[96]
	BS5-DOL0.5 (1:12.16 mol%)	0.1/-30	-95	-50–25	Zn	Li <sub>4</sub> Ti <sub>5</sub> O <sub>12</sub>	≈105@0.5 C	100	94	-20	[97]
	γ-Na <sub>1/3</sub> electrolyte	4.5/-30	-97	-50–80	Zn	PANI	≈79@0.125	≈800	—	-30	[68]
	Na-H <sub>2</sub> O-EG	3.9/-60	-72.6	-60–25	NaFeMnHCF	PTCDI	≈80@0.5 C	70	—	-60	[99]

Table 1. continued

Type of electrolytes	Electrolyte	Ionic conductivity [ $\text{mS cm}^{-1}$ ]	Freezing point [°C]	Operating temperature range [°C]	Anode	Cathode	Electrochemical performance	Cycles	Retention [%]	Temperature [°C]	Ref.
Water-in-salt electrolyte	$3.5 \text{ m Mg}(\text{ClO}_4)_2 + 0.5 \text{ m NaClO}_4$	4.86/-60	< -80	-60-25	active carbon	$\text{NaTi}_2(\text{PO}_4)_3\text{C}$	-@1.064	10000	-	-60	[100]
	LiPTFSI:LiOTf (15/5)	6.8/RT	-14	-10-25	Li	$\text{LiMn}_2\text{O}_4$	-@1 C	100	-	-10	[76]
	25 m NaFSI+10 m NaPTFSI	11.8/30	-34	-10-30	$\text{NaTi}_2(\text{PO}_4)_3$	$\text{Na}_3(\text{VOPO}_4)_2\text{F}$	-@0.2 C	500	83	-10	[75]
	17 M NaClO <sub>4</sub>	17/-40	-50	-40-25	-	-	-	-	-	-40	[77]
	$\text{Li}_2\text{ZnCl}_4\cdot 9\text{H}_2\text{O}$	$\approx 1.1/-70$	-110	-70-80	-	-	-	-	-	-	[101]
	MSE-1D W	1.58/-80	< -150	-80-25	Zn	PANI	71.8@0.5	3000	87	-80	[78]
	$\text{Zn}(\text{ClO}_4)_2\cdot 6\text{H}_2\text{O}/\text{SN}$ (1:8)	5.52/RT	< -90	-20-90	Zn	PDB	-@0.1	3500	85.4	25	[83a]
	SL+Zn( $\text{ClO}_4$ ) <sub>2</sub> ·6H <sub>2</sub> O (6:1)	0.1/-20	≈ -17	-40-25	Zn	PANI	73@0.3	500	-	-30	[83b]
Eutectic electrolyte	2-Propanol/H <sub>2</sub> O/Zn-(OTf) <sub>2</sub> (30 vol%)	-	< -100	-40-25	Zn	$\text{V}_2\text{O}_5$	≈ 175@1	2000	88.8	-20	[82]
	$3.5 \text{ M Mg}(\text{ClO}_4)_2 + 1 \text{ M Zn}(\text{ClO}_4)_2$	1.41/-70	-121	-70-25	Zn	PTO	101.5@0.2	100	-	-70	[83c]
	7.6 m ZnCl <sub>2</sub> +0.05 m SnCl <sub>2</sub>	0.8/-70	-118.15	-70-20	Zn	VOPO <sub>4</sub>	105.7@0.3 C	200	95	-50	[84]
	7.5 m ZnCl <sub>2</sub>	1.79/-60	-114	-90-60	Zn	PANI	84.9@0.2	2000	≈ 100	-70	[81]

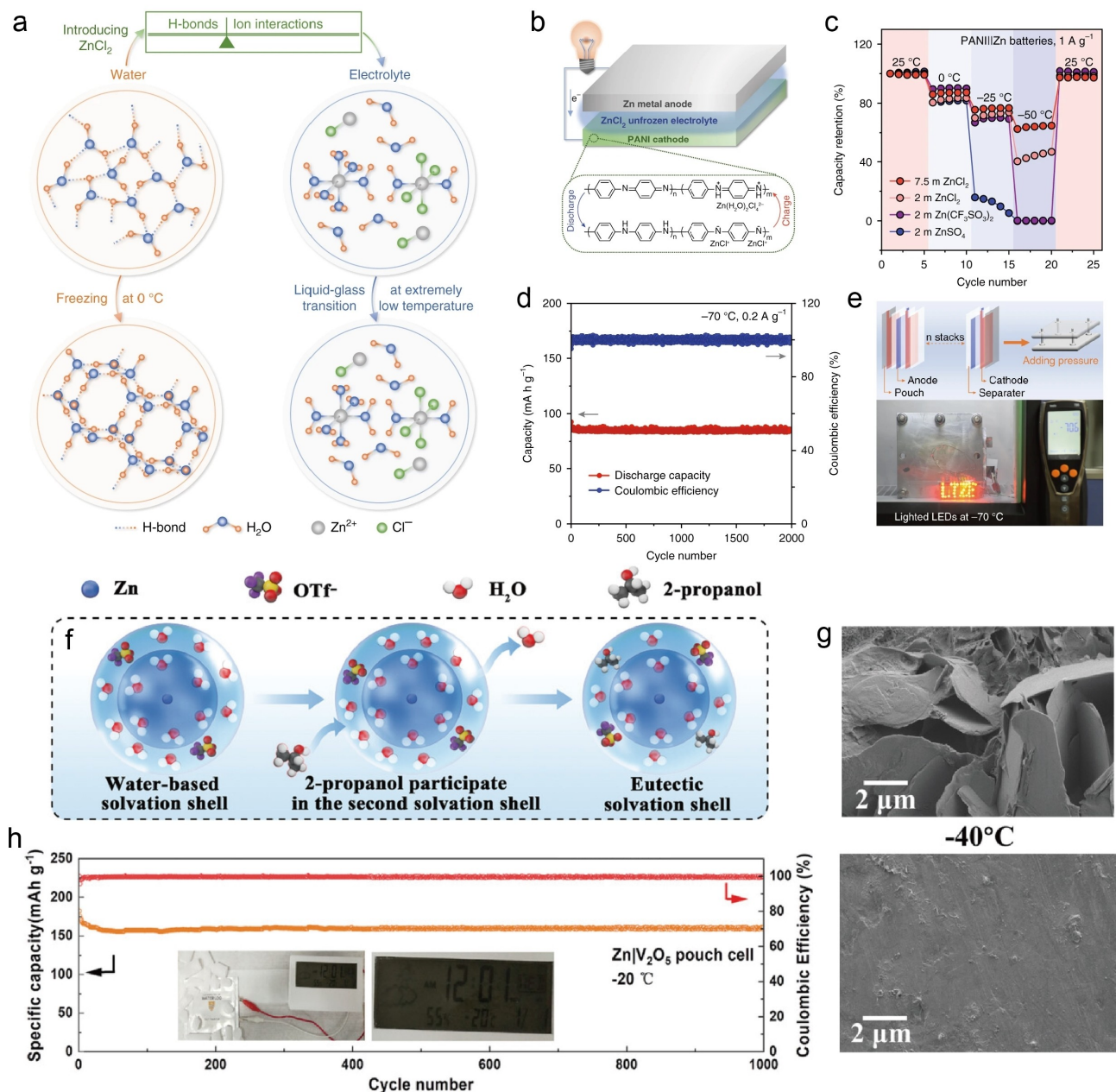


**Figure 11.** a) Schematic illustration of the structural evolution of water crystallization and design principles of water– $\text{ZnCl}_2$  electrolyte. b) Scheme of configuration and charge/discharge reaction of Zn/LTE/PANI batteries. c) Cycling performance of Zn/PANI cells from 25 °C to –50 °C. d) Cycling stability of Zn/LTE/PANI battery at –70 °C. e) Schematic of the pouch cell and the lighted LEDs at –70 °C. Reproduced with permission.<sup>[81]</sup> Copyright 2020, Springer Nature. f) Schematic illustration of the eutectic solvation shell. g) SEM images of Zn anode using electrolyte without 2-propanol and with addition of 2-propanol at –40 °C. h) Cycling performance of Zn/V<sub>2</sub>O<sub>5</sub> pouch cell with addition of 2-propanol at –20 °C. Reproduced with permission.<sup>[82]</sup> Copyright 2022, Wiley-VCH.

The combination of 2-propanol and  $\text{Zn}(\text{OTf})_2$  salt in research to improve low-temperature performance can be considered relatively environmentally friendly among eutectic electrolytes.<sup>[82]</sup> 2-Propanol is considered a green solvent compared to conventional solvents used in organic synthesis and is readily biodegradable.<sup>[86]</sup> In this study, 2-propanol was added to adjust the structure of the outer solvation shell of the Zn ion (Figure 11f). In this process, 2-propanol replaced water molecules to form a eutectic layer, which was found to have a significant impact on the Zn deposition morphology. Notably,

as the temperature decreased, the difference in morphology became more pronounced, with much more uniform Zn plating observed in the presence of 2-propanol (Figure 11g). Based on the effect of promoting uniform Zn growth at low-temperatures, a Zn/V<sub>2</sub>O<sub>5</sub> pouch cell achieved very stable operation over 2000 cycles at –20 °C (Figure 11h). Similar to WIS electrolytes, it is still challenging to completely replace the components of eutectic electrolytes with green materials, but as introduced in previous research, there is hope for future studies

to explore various directions, such as using sustainable materials as additives.

To provide a comprehensive overview, we summarized the key characteristics and performance of various batteries using the aqueous electrolytes for low-temperature applications (Table 1). This table includes information such as electrolyte composition, ionic conductivity, freezing points, operating temperature ranges, and electrochemical performance.

## 4. Summary and Outlook

Aqueous battery systems have received considerable attention as next-generation battery technologies due to their environmentally friendly characteristics. However, for commercialization, it is necessary to develop electrolytes that can operate stably at high voltages, and since these systems are water-based, they are also vulnerable to low-temperature operation. Various studies have been conducted to address these challenges, but some have used harmful materials that conflict with the environmentally friendly nature of AIBs. This review aims to highlight the need for research into green materials that can enhance the performance of aqueous batteries under both high voltage and low-temperature conditions.

Several issues can arise when increasing the operating voltage in aqueous electrolytes, primarily due to the narrow ESW of these electrolytes, leading to water decomposition or side reactions at high voltages. To overcome these challenges, various researches have been conducted in five areas of electrolytes: WIS electrolytes, WIBS electrolytes, molecular crowding electrolytes, eutectic electrolytes, and cosolvents for aqueous electrolytes. Each of these studies has successfully enabled high-voltage operation by effectively regulating the solvation structure of water.

Overall, along with the use of sustainable materials, these advancements have contributed significantly to the development of high-energy-density aqueous batteries capable of operating in a wider voltage range, paving the way for more efficient and sustainable aqueous battery technologies.

In low-temperature environments, the crystallization of water within aqueous electrolytes can significantly reduce the ionic conductivity, a major issue caused by the freezing of water molecules, leading to a rapid degradation of battery performance. To overcome these issues, four types of electrolyte systems—Hydrogel electrolytes, additives and cosolvents for electrolytes, WIS electrolytes, and eutectic electrolytes—have been studied. Each system has employed strategies using green materials such as beet extract and cotton-derived cellulose to weaken strong hydrogen bonds, thereby inhibiting water crystallization. This approach helps maintain excellent ionic conductivity even at low-temperatures, significantly lowering the freezing point and enabling the design of batteries that can operate reliably for long periods at subzero temperatures.

Green aqueous electrolytes face significant challenges, including lower ionic conductivity, limited chemical and electrochemical stability, and difficulties in scaling up for industrial applications. However, as demonstrated in this review, recent

advancements using sustainable materials show promise in overcoming these challenges, even under high-voltage and low-temperature conditions. By focusing on engineering advanced electrolyte materials with optimized solvation structures and novel salt formulations to improve both ionic conductivity and stability, we can envision a future where aqueous battery systems are both environmentally friendly and efficient. Continued progress in these green approaches will pave the way for the commercialization of aqueous batteries and significantly contribute to the development of sustainable energy systems.

## Acknowledgements

This study was supported by the Institute for Basic Science (project code: IBS-R006-A2). This work was supported by the Technology Innovation Program (Grant No. 20026752) funded by the Ministry of Trade, Industry & Energy (MOTIE, Korea). E. Park and J. Jeong contributed equally to this work.

## Conflict of Interests

The authors declare no competing interests.

**Keywords:** Anti-freezing • Aqueous ion batteries • Electrochemical stability window • Electrochemistry • Green electrolytes • Sustainable chemistry

- [1] European Commission, The European Green Deal, 2019.
- [2] a) K. Liu, Y. Liu, D. Lin, A. Pei, Y. Cui, *Sci. Adv.* **2018**, *4*, eaas9820; b) D. Larcher, J.-M. Tarascon, *Nat. Chem.* **2015**, *7*, 19–29.
- [3] a) R. Zalosh, P. Gandhi, A. Barowy, *J. Loss Prev. Process Indust.* **2021**, *72*, 104560; b) J. Weng, D. Ouyang, Y. Liu, M. Chen, Y. Li, X. Huang, J. Wang, *J. Power Sources* **2021**, *509*, 230340.
- [4] a) R. Fan, Z. Wang, Y. Lu, C. Lin, W. Guo, *Fuel* **2022**, *330*, 125450; b) A. W. Golubkov, D. Fuchs, J. Wagner, H. Wiltsche, C. Stangl, G. Fauler, G. Voitic, A. Thaler, V. Hacker, *RSC Adv.* **2014**, *4*, 3633–3642; c) V. Somandepalli, K. Marr, Q. Horn, *SAE Int. J. Altern. Powertrains* **2014**, *3*, 98–104.
- [5] X. Sun, H. Hao, F. Zhao, Z. Liu, *Resour. Conserv. Recycl.* **2017**, *124*, 50–61..
- [6] a) L. Li, X. Zhang, M. Li, R. Chen, F. Wu, K. Amine, J. Lu, *Electrochim. Energy Rev.* **2018**, *1*, 461–482; b) L. Gaines, *Sustain. Mater. Technol.* **2018**, *17*, e00068.
- [7] P. Kurzweil, *J. Power Sources* **2010**, *195*, 4424–4434..
- [8] T. Yamamoto, T. Shoji, *Inorg. Chim. Acta* **1986**, *117*, L27–L28..
- [9] W. Li, J. R. Dahn, D. S. Wainwright, *Science* **1994**, *264*, 1115–1118..
- [10] a) G. Fang, J. Zhou, A. Pan, S. Liang, *ACS Energy Lett.* **2018**, *3*, 2480–2501; b) C. Xu, B. Li, H. Du, F. Kang, *Angew. Chem. Int. Ed.* **2012**, *51*, 933–935.
- [11] M. Winter, R. J. Brodd, *Chem. Rev.* **2004**, *104*, 4245–4270.
- [12] a) J. F. Parker, C. N. Chervin, I. R. Pala, M. Machler, M. F. Burz, J. W. Long, D. R. Rolison, *Science* **2017**, *356*, 415–418; b) D. Kundu, B. D. Adams, V. Duffort, S. H. Vajargah, L. F. Nazar, *Nat. Energy* **2016**, *1*, 1–8.
- [13] J. Huang, Z. Guo, Y. Ma, D. Bin, Y. Wang, Y. Xia, *Small Methods* **2019**, *3*, 1800272.
- [14] a) H. Ahn, D. Kim, M. Lee, K. W. Nam, *Commun. Mater.* **2023**, *4*, 37; b) R. Wang, Q. Ma, L. Zhang, Z. Liu, J. Wan, J. Mao, H. Li, S. Zhang, J. Hao, L. Zhang, *Adv. Energy Mater.* **2023**, *13*, 2302543.
- [15] a) Y. H. Lee, Y. Jeoun, J. H. Kim, J. Shim, K. S. Ahn, S. H. Yu, Y. E. Sung, *Adv. Funct. Mater.* **2024**, *34*, 2310884; b) L. Zhang, J. Liu, Y. Zhai, S. Zhang, W. Wang, G. Li, L. Sun, H. Li, S. Qi, S. Chen, *Adv. Mater.* **2024**, *36*, 2313835.

- [16] N. Nicholls, D. Easterling, C. Goodess, S. Kanae, J. Kossin, Y. Luo, J. Marengo, K. McInnes, M. Rahimi, M. Reichstein, *Managing the risks of extreme events and disasters to advance climate change adaptation*, Cambridge University Press, Cambridge, UK, and New York, NY, USA, 2012.
- [17] D. Gielen, F. Boshell, D. Saygin, M. D. Bazilian, N. Wagner, R. Gorini, *Energy Strategy Rev.* 2019, 24, 38–50.
- [18] D. Chao, S.-Z. Qiao, *Joule* 2020, 4, 1846–1851.
- [19] M. Xia, H. Fu, K. Lin, A. M. Rao, L. Cha, H. Liu, J. Zhou, C. Wang, B. Lu, *Energy Environ. Sci.* 2024, 17, 1255–1265.
- [20] L. Suo, O. Borodin, T. Gao, M. Olguin, J. Ho, X. Fan, C. Luo, C. Wang, K. Xu, *Science* 2015, 350, 938–943.
- [21] M. Gu, H. Fu, A. M. Rao, J. Zhou, *Adv. Funct. Mater.* 2024, 2407867.
- [22] Y. Liang, Y. Yao, *Nat. Rev. Mater.* 2023, 8, 109–122.
- [23] M. R. Lukatskaya, J. I. Feldblyum, D. G. Mackanic, F. Lissel, D. L. Michels, Y. Cui, Z. Bao, *Energy Environ. Sci.* 2018, 11, 2876–2883.
- [24] J. Zheng, G. Tan, P. Shan, T. Liu, J. Hu, Y. Feng, L. Yang, M. Zhang, Z. Chen, Y. Lin, *Chem* 2018, 4, 2872–2882.
- [25] D. P. Leonard, Z. Wei, G. Chen, F. Du, X. Ji, *ACS Energy Lett.* 2018, 3, 373–374.
- [26] a) J. Han, A. Mariani, H. Zhang, M. Zarzabeitia, X. Gao, D. V. Carvalho, A. Varzi, S. Passerini, *Energy Stor. Mater.* 2020, 30, 196–205; b) T. Thomberg, R. Väli, J. Eskusson, T. Romann, A. Jänes, *J. Electrochem. Soc.* 2018, 165, A3862; c) D. Stępień, Z. Zhao, S. Dsoke, *J. Electrochem. Soc.* 2018, 165, A2807.
- [27] T. Liu, L. Tang, H. Luo, S. Cheng, M. Liu, *Chem. Commun.* 2019, 55, 12817–12820.
- [28] C. A. Angell, *J. Electrochem. Soc.* 1965, 112, 1224.
- [29] L. Suo, O. Borodin, W. Sun, X. Fan, C. Yang, F. Wang, T. Gao, Z. Ma, M. Schroeder, A. von Cresce, *Angew. Chem.* 2016, 128, 7252–7257.
- [30] S. Chen, R. Lan, J. Humphreys, S. Tao, *Energy Stor. Mater.* 2020, 28, 205–215.
- [31] D. Dong, T. Wang, Y. Sun, J. Fan, Y.-C. Lu, *Nat. Sustain.* 2023, 6, 1474–1484.
- [32] F. Wang, O. Borodin, T. Gao, X. Fan, W. Sun, F. Han, A. Faraone, J. A. Dura, K. Xu, C. Wang, *Nat. Mater.* 2018, 17, 543–549.
- [33] W. Kunz, K. Holmberg, T. Zemb, *Curr. Opin. Colloid Interface Sci.* 2016, 22, 99–107.
- [34] S.-i. Nakano, D. Miyoshi, N. Sugimoto, *Chem. Rev.* 2014, 114, 2733–2758.
- [35] J. Xie, Z. Liang, Y.-C. Lu, *Nat. Mater.* 2020, 19, 1006–1011.
- [36] Q. Nian, W. Zhu, S. Zheng, S. Chen, B.-Q. Xiong, Z. Wang, X. Wu, Z. Tao, X. Ren, *ACS Appl. Mater. Interfaces* 2021, 13, 51048–51056.
- [37] W. Chen, S. Guo, L. Qin, L. Li, X. Cao, J. Zhou, Z. Luo, G. Fang, S. Liang, *Adv. Funct. Mater.* 2022, 32, 2112609.
- [38] J. Ding, Q. Li, J. Yang, R. Wang, J. Ruan, F. Fang, D. Sun, F. Wang, *Adv. Funct. Mater.* 2024, 34, 2316295.
- [39] Q. Zhang, K. D. O. Vigier, S. Royer, F. Jérôme, *Chem. Soc. Rev.* 2012, 41, 7108–7146.
- [40] L. Geng, X. Wang, K. Han, P. Hu, L. Zhou, Y. Zhao, W. Luo, L. Mai, *ACS Energy Lett.* 2021, 7, 247–260.
- [41] D. Feng, F. Cao, L. Hou, T. Li, Y. Jiao, P. Wu, *Small* 2021, 17, 2103195.
- [42] Y. Zhong, X. Xie, Z. Zeng, B. Lu, G. Chen, J. Zhou, *Angew. Chem. Int. Ed.* 2023, 62, e202310577.
- [43] C. Lu, Z. Wang, Y. Zhang, G. Tang, Y. Wang, X. Guo, J. Li, L. Wei, *Nano Energy* 2024, 120, 109158.
- [44] Y. Gu, F. Jérôme, *Green Chem.* 2010, 12, 1127–1138.
- [45] X. Zhang, R. Wang, Z. Liu, Q. Ma, H. Li, Y. Liu, J. Hao, S. Zhang, J. Mao, C. Zhang, *Adv. Energy Mater.* 2024, 14, 2400314.
- [46] J. Wan, R. Wang, Z. Liu, S. Zhang, J. Hao, J. Mao, H. Li, D. Chao, L. Zhang, C. Zhang, *Adv. Mater.* 2024, 36, 2310623.
- [47] Z. Su, J. Chen, W. Ren, H. Guo, C. Jia, S. Yin, J. Ho, C. Zhao, *Small* 2021, 17, 2102375.
- [48] Z. Li, Y. Liao, Y. Wang, J. Cong, H. Ji, Z. Huang, Y. Huang, *Energy Stor. Mater.* 2023, 56, 174–182.
- [49] F. Ming, Y. Zhu, G. Huang, A.-H. Emwas, H. Liang, Y. Cui, H. N. Alshareef, *J. Am. Chem. Soc.* 2022, 144, 7160–7170.
- [50] L. Miao, R. Wang, W. Xin, L. Zhang, Y. Geng, H. Peng, Z. Yan, D. Jiang, Z. Qian, Z. Zhu, *Energy Stor. Mater.* 2022, 49, 445–453.
- [51] Y. Wang, T. Ou, Y. Dong, L. Chen, Y. Huang, D. Sun, W. Qiang, X. Pei, Y. Li, Y. Tan, *Adv. Mater.* 2024, 36, 2311009.
- [52] S. I. Zandalinas, F. B. Fritsch, R. Mittler, *Trends Plant Sci.* 2021, 26, 588–599.
- [53] K. Guo, S. Qi, H. Wang, J. Huang, M. Wu, Y. Yang, X. Li, Y. Ren, J. Ma, *Small Sci.* 2022, 2, 2100107.
- [54] Y. Zhao, Z. Chen, F. Mo, D. Wang, Y. Guo, Z. Liu, X. Li, Q. Li, G. Liang, C. Zhi, *Adv. Sci.* 2021, 8, 2002590.
- [55] a) M. S. Ding, A. von Cresce, K. Xu, *J. Phys. Chem. C* 2017, 121, 2149–2153; b) J. H. Park, N. Aluru, *Mol. Simul.* 2009, 35, 31–37.
- [56] E. M. Ahmed, *J. Adv. Res.* 2015, 6, 105–121.
- [57] Z. Liu, X. Luo, L. Qin, G. Fang, S. Liang, *Adv. Powder Mater.* 2022, 1, 100011.
- [58] M. Zhu, X. Wang, H. Tang, J. Wang, Q. Hao, L. Liu, Y. Li, K. Zhang, O. G. Schmidt, *Adv. Funct. Mater.* 2020, 30, 1907218.
- [59] H. Lu, J. Hu, L. Wang, J. Li, X. Ma, Z. Zhu, H. Li, Y. Zhao, Y. Li, J. Zhao, *Adv. Funct. Mater.* 2022, 32, 2112540.
- [60] R. Wang, M. Yao, S. Huang, J. Tian, Z. Niu, *Sci. China Mater.* 2022, 65, 2189–2196.
- [61] M. Martí, L. Molina, C. Aleman, E. Armelin, *ACS Sustain. Chem. Eng.* 2013, 1, 1609–1618.
- [62] S. Huang, S. He, Y. Li, S. Wang, X. Hou, *Chem. Eng. J.* 2023, 464, 142607.
- [63] F. Mo, G. Liang, D. Wang, Z. Tang, H. Li, C. Zhi, *EcoMat* 2019, 1, e12008.
- [64] M. Chen, J. Chen, W. Zhou, X. Han, Y. Yao, C. P. Wong, *Adv. Mater.* 2021, 33, 2007559.
- [65] Y. Q. Jiang, J. Li, Z. W. Feng, G. Q. Xu, X. Shi, Q. J. Ding, W. Li, C. H. Ma, B. Yu, *Adv. Synth. Catal.* 2020, 362, 2609–2614.
- [66] N. Wang, Y. Yang, X. Qiu, X. Dong, Y. Wang, Y. Xia, *ChemSusChem* 2020, 13, 5556–5564.
- [67] A. Wolfson, C. Dlugy, Y. Shotland, *Environ. Chem. Lett.* 2007, 5, 67–71.
- [68] F. Wang, O. Borodin, M. S. Ding, M. Gobet, J. Vatamanu, X. Fan, T. Gao, N. Eidson, Y. Liang, W. Sun, *Joule* 2018, 2, 927–937.
- [69] Q. Zhang, K. Xia, Y. Ma, Y. Lu, L. Li, J. Liang, S. Chou, J. Chen, *ACS Energy Lett.* 2021, 6, 2704–2712.
- [70] D. S. Liu, Y. Zhang, S. Liu, L. Wei, S. You, D. Chen, M. Ye, Y. Yang, X. Rui, Y. Qin, *Adv. Funct. Mater.* 2022, 32, 2111714.
- [71] T. Jin, X. Ye, Z. Chen, S. Bai, Y. Zhang, *ACS Appl. Mater. Interfaces* 2024, 16, 4729–4740.
- [72] N. Yabueng, S. C. Napaphorn, *Process Biochem.* 2018, 69, 197–207.
- [73] T. Wei, Y. Peng, L.-e. Mo, S. Chen, R. Ghadari, Z. Li, L. Hu, *Sci. China Mater.* 2022, 65, 1156–1164.
- [74] H. Ren, S. Li, B. Wang, Y. Zhang, T. Wang, Q. Lv, X. Zhang, L. Wang, X. Han, F. Jin, *Adv. Mater.* 2023, 35, 2208237.
- [75] D. Reber, *ACS Mater. Lett.* 2019, 1, 44–51.
- [76] M. Becker, R.-S. Künnel, C. Battaglia, *Chem. Commun.* 2019, 55, 12032–12035.
- [77] X. Wang, H. Huang, F. Zhou, P. Das, P. Wen, S. Zheng, P. Lu, Y. Yu, Z.-S. Wu, *Nano Energy* 2021, 82, 105688.
- [78] J. Yao, B. Zhang, X. Wang, L. Tao, J. Ji, Z. Wu, X. Liu, J. Li, Y. Gan, J. Zheng, *Angew. Chem.* 2024, 09986, e2024.
- [79] a) Y. Zhao, Y. Kang, H. Du, F. Kang, B. Li, *J. Energy Chem.* 2024, 93, 46–54; b) J. Lin, X. Zhang, E. Fan, R. Chen, F. Wu, L. Li, *Energy Environ. Sci.* 2023, 16, 745–791.
- [80] Q. Nian, T. Sun, S. Liu, H. Du, X. Ren, Z. Tao, *Chem. Eng. J.* 2021, 423, 130253.
- [81] Q. Zhang, Y. Ma, Y. Lu, L. Li, F. Wan, K. Zhang, J. Chen, *Nat. Commun.* 2020, 11, 4463.
- [82] Q. Ma, R. Gao, Y. Liu, H. Dou, Y. Zheng, T. Or, L. Yang, Q. Li, Q. Cu, R. Feng, *Adv. Mater.* 2022, 34, 2207344.
- [83] a) W. Yang, X. Du, J. Zhao, Z. Chen, J. Li, J. Xie, Y. Zhang, Z. Cui, Q. Kong, Z. Zhao, *Joule* 2020, 4, 1557–1574; b) X. Lin, G. Zhou, M. J. Robson, J. Yu, S. C. Kwok, F. Ciucci, *Adv. Funct. Mater.* 2022, 32, 2109322; c) T. Sun, S. Zheng, H. Du, Z. Tao, *Nano-Micro Lett.* 2021, 13, 1–10.
- [84] L. Cao, D. Li, F. A. Soto, V. Ponce, B. Zhang, L. Ma, T. Deng, J. M. Seminario, E. Hu, X. Q. Yang, *Angew. Chem. Int. Ed.* 2021, 60, 18845–18851.
- [85] a) F. Gschwind, H. Euchner, G. Rodriguez-Garcia, *Eur. J. Inorg. Chem.* 2017, 2017, 2784–2799; b) R. Corral-Higuera, S. P. Arredondo-Rea, M. Neri-Flores, J. Gómez-Solerón, J. L. Almaral-Sánchez, J. Castorena-González, A. Martínez-Villafañe, F. Almeraya-Calderón, *Int. J. Electrochem. Sci.* 2011, 6, 958–970.
- [86] a) R. A. Sheldon, *Curr. Opin. Green Sustain. Chem.* 2019, 18, 13–19; b) M. Bustard, E. McEvoy, J. Goodwin, J. Burgess, P. Wright, *Appl. Microbiol. Biotechnol.* 2000, 54, 424–431.
- [87] Y. Sun, Y. Zhang, Z. Xu, W. Gou, X. Han, M. Liu, C. M. Li, *ChemSusChem* 2022, 15, e202201362.
- [88] A. Tron, S. Jeong, Y. D. Park, J. Mun, *ACS Sustain. Chem. Eng.* 2019, 7, 14531–14538.
- [89] S. Huang, L. Hou, T. Li, Y. Jiao, P. Wu, *Adv. Mater.* 2022, 34, 2110140.

- [90] W. Zhou, J. Chen, M. Chen, A. Wang, A. Huang, X. Xu, J. Xu, C.-P. Wong, *J. Mater. Chem. A* **2020**, *8*, 8397–8409.
- [91] X. Li, H. Wang, X. Sun, J. Li, Y.-N. Liu, *ACS Appl. Energy Mater.* **2021**, *4*, 12718–12727.
- [92] M. Chen, W. Zhou, A. Wang, A. Huang, J. Chen, J. Xu, C.-P. Wong, *J. Mater. Chem. A* **2020**, *8*, 6828–6841.
- [93] J. Liu, C. Yang, X. Chi, B. Wen, W. Wang, Y. Liu, *Adv. Funct. Mater.* **2022**, *32*, 2106811.
- [94] B. Niu, Z. Li, D. Luo, X. Ma, Q. Yang, Y.-E. Liu, X. Yu, X. He, Y. Qiao, X. Wang, *Energy Environ. Sci.* **2023**, *16*, 1662–1675.
- [95] N. Chang, T. Li, R. Li, S. Wang, Y. Yin, H. Zhang, X. Li, *Energy Environ. Sci.* **2020**, *13*, 3527–3535.
- [96] G. Yang, J. Huang, X. Wan, B. Liu, Y. Zhu, J. Wang, O. Fontaine, S. Luo, P. Hiralal, Y. Guo, *EcoMat* **2022**, *4*, e12165.
- [97] Z. Ma, J. Chen, J. Vatamanu, O. Borodin, D. Bedrov, X. Zhou, W. Zhang, W. Li, K. Xu, L. Xing, *Energy Stor. Mater.* **2022**, *45*, 903–910.
- [98] C. Xie, S. Liu, H. Wu, Q. Zhang, C. Hu, Z. Yang, H. Li, Y. Tang, H. Wang, *Sci. Bull.* **2023**, *68*, 1531–1539.
- [99] L. Jiang, S. Han, Y.-C. Hu, Y. Yang, Y. Lu, Y.-C. Lu, J. Zhao, L. Chen, Y.-S. Hu, *Nat. Energy* **2024**, *9*, 839–848.
- [100] K. Zhu, Z. Sun, T. Jin, X. Chen, Y. Si, H. Li, L. Jiao, *Batter. Supercaps* **2022**, *5*, e202200308.
- [101] C. Yang, J. Xia, C. Cui, T. P. Pollard, J. Vatamanu, A. Faraone, J. A. Dura, M. Tyagi, A. Kattan, E. Thimsen, *Nat. Sustain.* **2023**, *6*, 325–335.

Manuscript received: August 31, 2024  
Revised manuscript received: September 25, 2024  
Accepted manuscript online: September 26, 2024  
Version of record online: November 6, 2024